TECHNICAL REPORT
NATICK/TR-10/017

AD _____

DEVELOPMENT OF AN ADVANCED FLAMELESS COMBUSTION HEAT SOURCE UTILIZING METHANOL

by
Clifford G. Welles

Catalytic Devices International, LLC
Pleasanton, CA 94588

July 2010

Final Report
December 2002 – November 2003

Approved for public release; distribution is unlimited.

Prepared for
U.S. Army Natick Soldier Research, Development and Engineering Center
Natick, Massachusetts 01760-5018

UNCLASSIFIED

DISCLAIMERS

The findings contained in this report are not to be construed as an official Department of the Army position unless so designated by other authorized documents.

Citation of trade names in this report does not constitute an official endorsement or approval of the use of such items.

DESTRUCTION NOTICE

For Classified Documents:

Follow the procedures in DoD 5200.22-M, Industrial Security Manual, Section II-19 or DoD 5200.1-R, Information Security Program Regulation, Chapter IX.

For Unclassified/Limited Distribution Documents:

Destroy by any method that prevents disclosure of contents or reconstruction of the document.

REPORT DOCUMENTATION PAGE

Form Approved
OMB No. 0704-0188

PLEASE DO NOT RETURN YOUR FORM TO THE ABOVE ADDRESS.

1. REPORT DATE *(DD-MM-YYYY)*	2. REPORT TYPE	3. DATES COVERED *(From - To)*
07-07-2010	Final	December 2002 - November 2003

4. TITLE AND SUBTITLE

DEVELOPMENT OF AN ADVANCED FLAMELESS COMBUSTION HEAT SOURCE UTILIZING METHANOL

5a. CONTRACT NUMBER
DAAD16-03-C-0002-P00001

5b. GRANT NUMBER

5c. PROGRAM ELEMENT NUMBER
622786

6. AUTHOR(S)

Clifford G. Welles

5d. PROJECT NUMBER

5e. TASK NUMBER

5f. WORK UNIT NUMBER

7. PERFORMING ORGANIZATION NAME(S) AND ADDRESS(ES)

Catalytic Devices International, LLC
7063-E Commerce Circle
Pleasanton, CA 94588

8. PERFORMING ORGANIZATION REPORT NUMBER

9. SPONSORING / MONITORING AGENCY NAME(S) AND ADDRESS(ES)

U.S. Army Natick Soldier Research, Development and Engineering Center
ATTN: RDNS-CFE (A. Schmidt)
Kansas Street, Natick, MA 01760-5018

10. SPONSOR/MONITOR'S ACRONYM(S)

11. SPONSOR/MONITOR'S REPORT NUMBER(S)
NATICK/TR-10/017

12. DISTRIBUTION / AVAILABILITY STATEMENT

Approved for public release; distribution is unlimited.

13. SUPPLEMENTARY NOTES

14. ABSTRACT

Report developed under Broad Agency Announcement contract. As part of ongoing efforts to provide soldiers with easier and faster methods for heating water, food and themselves, while simultaneously decreasing fuel consumption and bulk, and as an alternative to open-flame stoves or chemical heaters, Catalytic Devices International, LLC (CDI) was awarded a Broad Agency Announcement (BAA) contract to develop a fundamentally new type of heating device. The company partnered with, and received 50% matching funding from a major commercial outdoor-equipment manufacturer interested in the technology for camping food and installation in clothing. This report summarizes the effort spanning December 2002 to November 2003. It notes the technical obstacles, solutions, new approaches taken in adapting the Advanced Flameless Combustion Technology (AFCT) principles toward practical application.

15. SUBJECT TERMS

FUELS	HAZARDS	CHEMICAL HEATERS	
WATER	CATALYSIS	VAPORIZATION	FUEL CONSUMPTION
STOVES	EFFICIENCY	SYSTEM DESIGN	FEASIBILITY STUDIES
FLAMES	METHANOLS	SAFETY FACTORS	FLAMELESS COMBUSTION
RATIONS	PROTOTYPES	COOKING DEVICES	FLAMELESS RATION HEATERS
HEATING	COMBUSTION	HEATING ELEMENTS	

16. SECURITY CLASSIFICATION OF:			17. LIMITATION OF ABSTRACT	18. NUMBER OF PAGES	19a. NAME OF RESPONSIBLE PERSON
a. REPORT	b. ABSTRACT	c. THIS PAGE			Alex Schmidt
U	U	U	SAR	76	19b. TELEPHONE NUMBER *(include area code)* (508) 233-6042

Standard Form 298 (Rev. 8-98)
Prescribed by ANSI Std. Z39.18

This page intentionally left blank

Table of Contents

List of Figures

List of Tables

Preface

As part of ongoing efforts to provide soldiers with easier and faster methods for heating water, food and themselves, while simultaneously decreasing fuel consumption and bulk, and as an alternative to open-flame stoves or chemical heaters, Catalytic Devices International, LLC (CDI) was awarded Broad Agency Announcement (BAA) contract #DAAD16-03-C-0002-P00001to develop a fundamentally new type of heating device. The company partnered with and received 50% matching funding from a major commercial outdoor-equipment manufacturer interested in the technology for camping food and installation in clothing. The contract was awarded by the U.S. Army Natick Soldier Research, Development and Engineering Center (NSRDEC), program element number 622786.

This report summarizes CDI's efforts under the contract, spanning December 2002 to November 2003. It notes the technical obstacles, solutions, new approaches taken in adapting the Advanced Flameless Combustion Technology (AFCT) principles toward practical application.

The goal is to achieve catalytic heat generation of at least 100 watts (340 BTU/hr) within thin, lightweight, flexible sheets based on the application of unique catalytic reaction and control principles established and patented by CDI. This will be carried out by integrating individual sub-system components, which have been separately studied and advanced in earlier work, into a single prototype heating unit that will demonstrate the attributes of AFCT with regard to commercial and specific military applications. The concept system consists of a combined fuel storage/vaporizer cartridge about the size of a cigarette pack that delivers a fuel/air mixture to catalyst-coated plastic sheets for a controlled, low-temperature flameless combustion with uniform distribution of heat. The plastic sheets are flexible and formable to virtually any shape.

The project effort was divided into two phases. Progress toward achieving specific milestones during each phase was the primary measure of the project's achievements. The major milestones for phase 1 were:

(1) a breadboard demonstration of the basic functionality of the technology without establishing specific form or fit factors.

(2) a brassboard demonstration of a methanol-based device, roughly 20x20 cm and 0.4 cm thick, capable of at least 100 watts of heat energy output. Much of the form and fit factors were incorporated into the device at this milestone, including electronic controls that are refined in both power consumption and size.

The major milestones for phase 2 were:

(1) enhancements to the subsystems to allow for reliable & portable operation.

(2) performing "best of breed" selection process for subsystems.

(3) demonstration of a fully integrated Meal, Ready-to-Eat (MRE) catalytic heater.

This project addresses the Combat Rations for Enhanced War fighter Logistics (CREWL) Science and Technology Objective (STO/DTO) which includes the Remote Unit Self-Heating Meal (RUSHM). It was accepted as a Joint Service Need (JSN) at the 2001 April review. Objective Force Warrior (OFW) has expressed interest and provided some co-funding because of the technology's application to boots, gloves and clothing for the individual soldier.

The citation of trade names in this report does not imply endorsement or any other approval of said products by the Government.

This page intentionally left blank

DEVELOPMENT OF AN ADVANCED FLAMELESS COMBUSTION HEAT SOURCE UTILIZING METHANOL

1. Summary

Catalytic Devices International, LLC (CDI) was awarded a Broad Agency Announcement (BAA) contract by the U.S. Army Natick Soldier Research, Development and Engineering Center (NSRDEC) to develop a fundamentally new type of heating device. This report summarizes the efforts by CDI under that contract, spanning December 2002 to November 2003.

During the first phase of this development effort, the scope was expanded to include certain potentially enabling technologies not originally anticipated as part of the development. This was done as a means of mitigating technical risk. By expanding the scope, the *schedule* risk was naturally increased, but this was considered preferable to ignoring the consequences of a technical failure.

In particular, three technical development activities were expanded beyond the original plan. These were the (a) electronic system design, (b) the fuel metering and vaporization, and (c) the temperature sensing array. The first two resulted from concern over achieving adequate fuel vaporization (i.e., power output goals) in a cost effective manner. The last one results from a failure of the original planned approach to make suitable quality, screened-on thermistors.

Overall, excellent progress was obtained toward the goal of achieving a well-controlled, spatially uniform, low-temperature catalytic heat producing reaction.

Primary Achievements for Phase 1

(1) Developed controlling algorithms, electronics system designs and miniaturized electronics hardware to implement control of two separate fuel-vaporization schemes. In particular, the thermal ink-jet (TIJ) vaporizer and a type of forced air evaporation technique known as the vapor extraction membrane (VEM) vaporizer.

(2) Developed a TIJ vaporizer to the point where it is capable of operating with a single head at a heat output power of 50 watts. Completed a design for a dual head TIJ capable of 100 watts (340 BTU/hour) output in a new slim-line fuel module.

(3) Developed a VEM fuel vaporizer capable of 300 watts (1025 BTU/hour) of heat energy output.

(4) Developed a high efficiency rotary-vane air pump capable of delivering 5-liter/minute air flow at less than 600 milliwatts power consumption.

Primary Achievements for Phase 2

(1) Redesigned the temperature sensing array to allow the use of inexpensive surface mount thermistors. This allowed heat-sheet surface temperature to safely reach 200°C. This

proved to be robust and maintain a good precision over time. Alternative methods were examined, but were judged too exploratory for this phase of the project.

(2) A dual-head TIJ unit was developed that had 100 watts of thermal power output and an automatic priming mechanism technique.

(3) An advanced vapor extraction membrane (VEM) vaporizer was developed using a newer less expensive, vapor extraction membrane structure. In particular, a way was discovered to replace the tubular e-PTFE (polytetrafluoroethylene, also known as Teflon) membranes with ribbon-like oleophobic membranes. These new membranes allowed an increase in the molar concentration of methanol to the 100% level and substantially reduced the cost and assembly time of a vaporization unit.

(4) Practical and theoretical ways to improve the "natural" stability (i.e., tendency for the reaction front to collapse) of the flameless heat process were developed. Catalytic heat elements were constructed using a new method that improved repeatability and temperature-uniformity along the length of the heat element.

(5) Catalytic heat-sheet development was continued to the point where lightweight, thin and flexible sheets were achieved

(6) A "best of breed" trade-off between all subsystem variations was performed and resulted in using these subsystems to demonstrate a portable catalytic MRE heater.

Table 1 illustrates the scheduled project milestones, as well as the major development activities needed to meet the planned timing for demonstration of a breadboard and brassboard system.

Table 1. AFCT Development Time Line - Phase 1

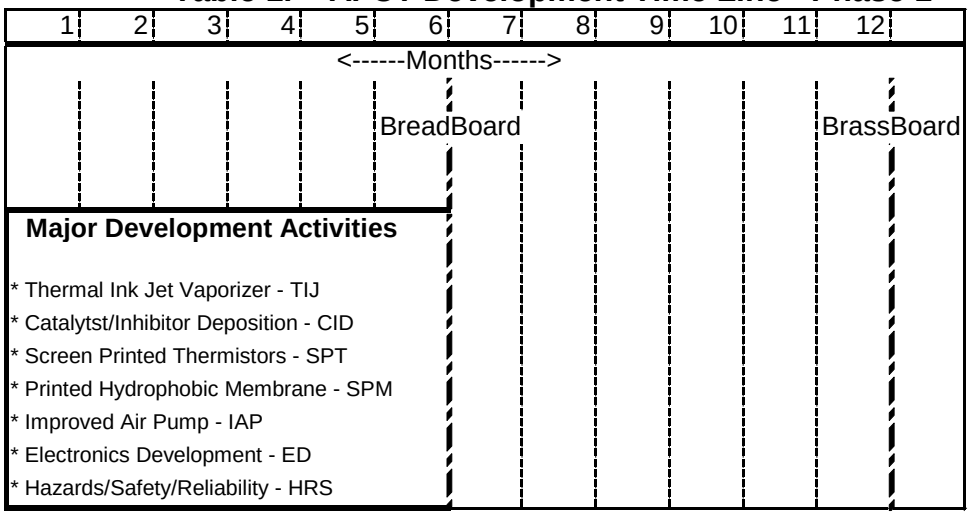

The purpose of the breadboard milestone is to provide basic function without concern for form factors, fit factors or overall ruggedness.

Analysis of the performance of the breadboard allowed corrections to the various subsystems that comprise a complete device. This included but is not limited to:

(a) modifying the control algorithm;
(b) modifying the construction process (e.g., heat sheet lamination, heat element construction, etc.); and
(c) modifying the fuel delivery sub-system (i.e., TIJ unit or VEM unit).

This provided the groundwork necessary for construction of the brassboard prototype.

The purpose of the brassboard prototype is to provide basic function along with critical form and fit factors necessary to perform well in the intended application. In the process of constructing the brassboard version, CDI determined what worked well, or not so well, and therefore new technical directions for the phase 2 effort.

The details leading to the breadboard and brassboard milestones for phase 1 are discussed in section 2.

The many additional refinements necessary to achieve an engineering prototype were planned for phase 2. These additional development activities are shown in **Table 2**.

Table 2. AFCT Development Time Line - Phase 2

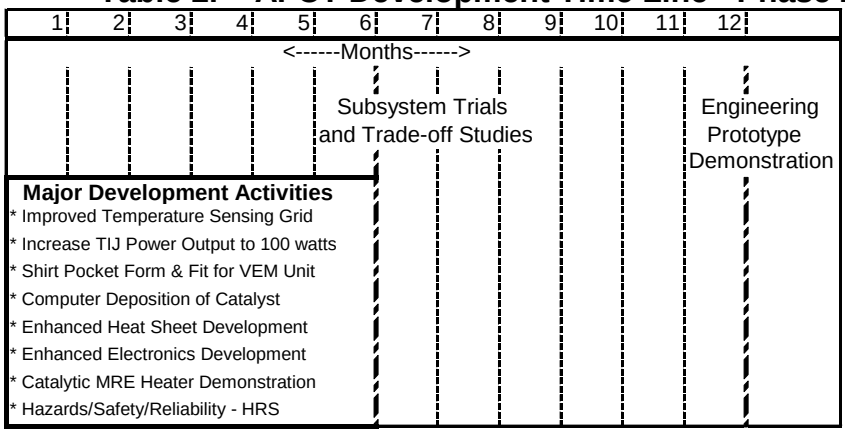

Demonstration of the engineering prototype was accomplished after a series of "best-of-breed" trade-off trials were performed to determine which subsystem designs best suited the intended application.

2. Phase 1 Development Activities

2.1 Electronics System Design

The principal control electronic functions for AFCT may be categorized according to (a) system monitoring, (b) user interface, and (c) controlling fuel and air metering based on inputs from system monitoring and user interface.

The monitoring function is both a safety task as well as a flameless combustion control task. Depending on the choice of techniques for fuel and air metering (e.g., TIJ, VEM, thermo-capillary, etc.) the process monitoring the data is used to insure optimum values for the fuel-to-air ratio and the total equivalent chemical power in the flow stream.

Part of the success of the combustion control algorithm is determined by the spatial temperature profiles across the catalytic heat elements and the maximum temperature limits experienced -- see, for instance, the temperature profiles shown in section 2.5.

Figure 1 illustrates the control hierarchy used by AFCT. It can be seen that the item to be heated (e.g., heat sheet) contains temperature sensors and impulse starter resistors (i.e., to produce a transient heat pulse to start the flameless combustion process).

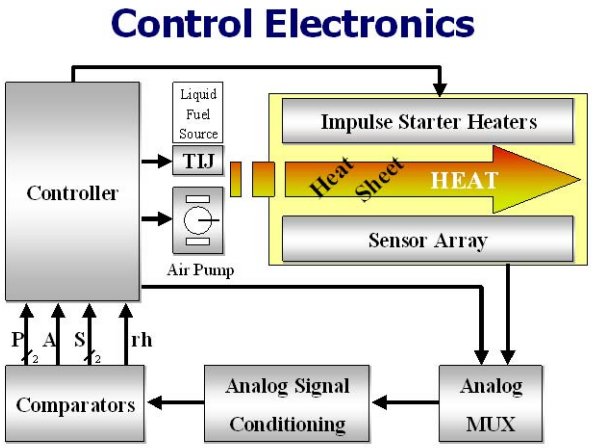

Figure 1. Controller Block Diagram

The controller uses this information and its spatial distribution to determine what the fuel and air metering values should be. The signal conditioning circuit extracts peak (P), average (A) and spatial symmetry values from the temperature sensors. Reheat (rh) commands for the starter resistors are also determined from this information and used to insure the heat elements are always in a reactive state except during shutdown mode. During cold conditions it is sometimes necessary to send a short electrical pulse (one second) to the starters to insure a rapid start-up.

Figure 2 further illustrates the design philosophy by emphasizing the potential for AFCT to be in a state of relatively unstable equilibrium. That is, the reaction front can drift in position over time depending on the design features of the heat elements.

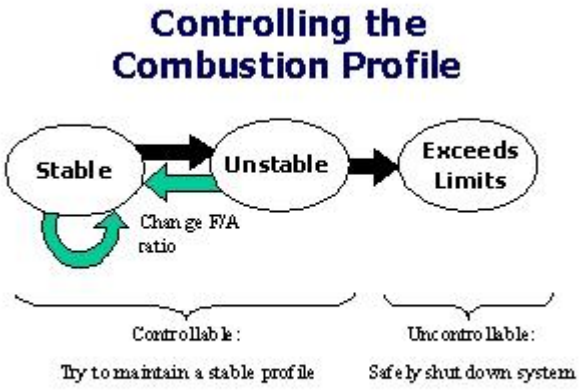

Figure 2. Control Philosophy

In the first phase of the development program, emphasis was placed on anticipating an unstable equilibrium, but the second phase effort (section 3) improvements in the repeatability of heat element design increased the intrinsic stability reaction of the heat elements so that they are naturally stable, lessening the demands of the control electronics and reducing overall costs.

By way of contrast, if the completely passive approach to catalytic heat, sometimes known as membrane diffusive (pioneered and patented by CDI) has been selected as the core technology, electronic control would still be the only prudent approach. This is because, all heat sources that come into close personal contact with the body on a regular basis can be enhanced in terms of safety by incorporating even a rudimentary electronic control system. It will make approval by the responsible regulating agencies much less problematic and limit liability issues.

Figure 3, **Figure 4** and **Figure 5** provide more details regarding the objectives of the state machine program and the logic look-up-table encoded in the complex programmable logic device (CPLD) that is the heart of the controller.

In the first phase, CDI chose to center the design of the VEM-driven cooking application on an Atmel 1504 chip, and the TIJ-driven application on an Amtel 1508 chip, because the VEM application requires much less complex control and monitoring.

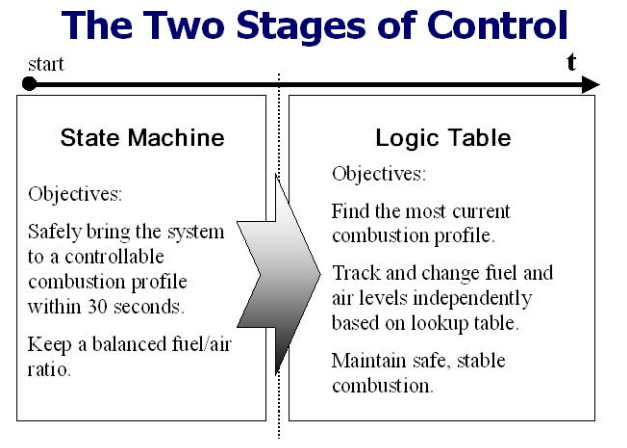

Figure 3. Control Methodology (Part I)

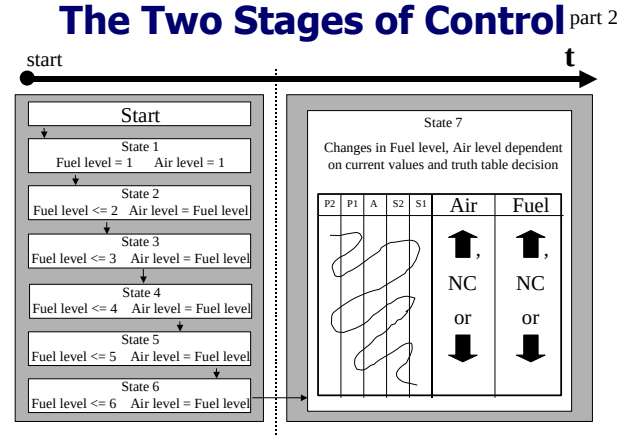

Figure 4. Control Methodology (Part II)

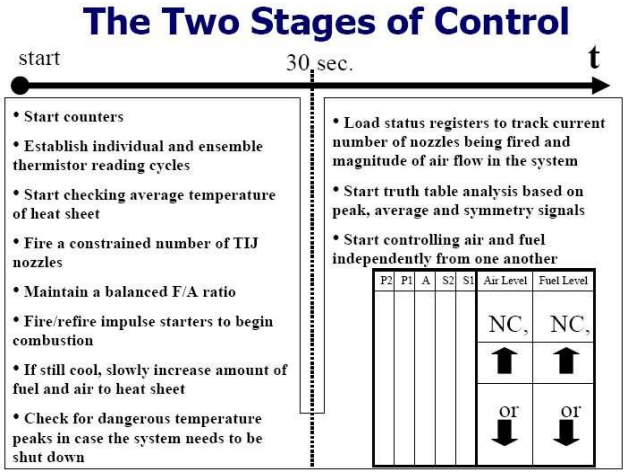

Figure 5. Control Methodology (Part III)

In the second phase, CDI redesigned the electronics, explored design centered on both the Xilinx (ultra-low power consumption) CPLD and a small micro control unit (MCU) device, the purpose being to reduce the electronics cost further by employing a small macrocell CPLD and a small MCU, the total cost of which is less than half the cost of the single large macrocell CPLD currently being used. For non-TIJ based evaporation subsystems, only the MCU need be considered.

Because currently considered applications need to be portable, reliance on batteries was anticipated and designed into the early prototypes. Key to successful portable operation, however, is the efficient use of battery energy. Miniature DC/DC switcher circuits were used in phase 1 to achieve the required voltage levels of each electronic subsystem. Each required specific switcher topologies that were the only way to accurately gauge battery life. **Figure 6** shows the diagrammatic set-up for the test.

The initial design for the control electronics calls for two DC/DC switcher supplies as shown in Figure 6. The reason for this has to do with the large difference in power and voltage demands for each of the controller subcircuits. Handling all of these loads properly and keeping the conversion efficiency high while requiring a range battery voltages that span 1.8 V to 3 V, is a major challenge.

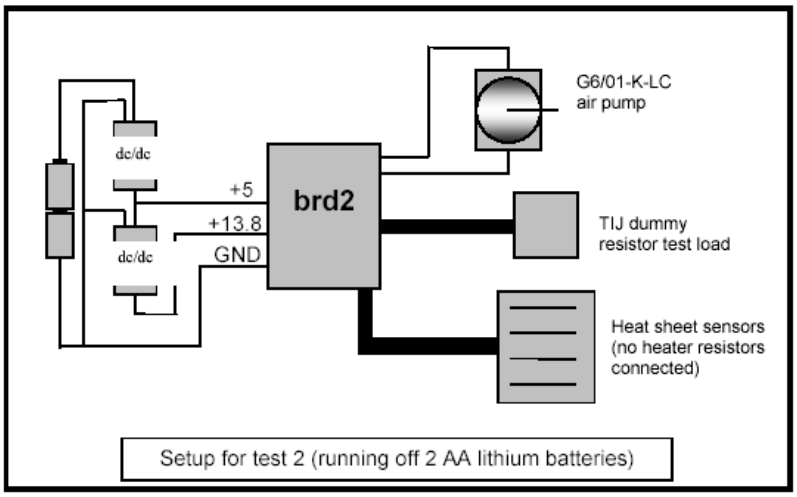

Figure 6. Bench Test Set-up for DC-DC Battery Life Test

The battery life test revealed that two AA lithium iron disulfide cells (i.e., 1.5 volts each) could drive the system for 6 hours while simulating a maximum output operating condition. If the unit is allowed to run intermittently, say one hour on and 1 hour off, then it is expected the lifetime would be several hours longer. The near-term design goal is to achieve 13 hours of continuously running battery life from the two AA batteries mentioned above. This is expected to result from increased efficiency of the converters and improved efficiency of the air pump.

Based on projected improvements for future designs, it is anticipated that 20 to 30 hours of operational time can eventually be expected from these batteries (or batteries of similar energy density) during normal operation. The batteries could be either rechargeable or primary cells depending on the application.

Figure 7 and **Figure 8** show the latest design revisions for the two separate fuel/air vaporization schemes. The Figure 7 circuit diagram is designed to drive either one or two TIJ heads simultaneously. It is intended to operate with a heat sheet that has a sensor grid attached. The sensor information is then used to decide how much air and fuel is needed at any time to maintain a stable and uniform reaction front during the flameless combustion process.

In Figure 8 it can be seen that a more simplified circuitry can be used with the VEM-type vaporizers, lowering costs and improving reliability.

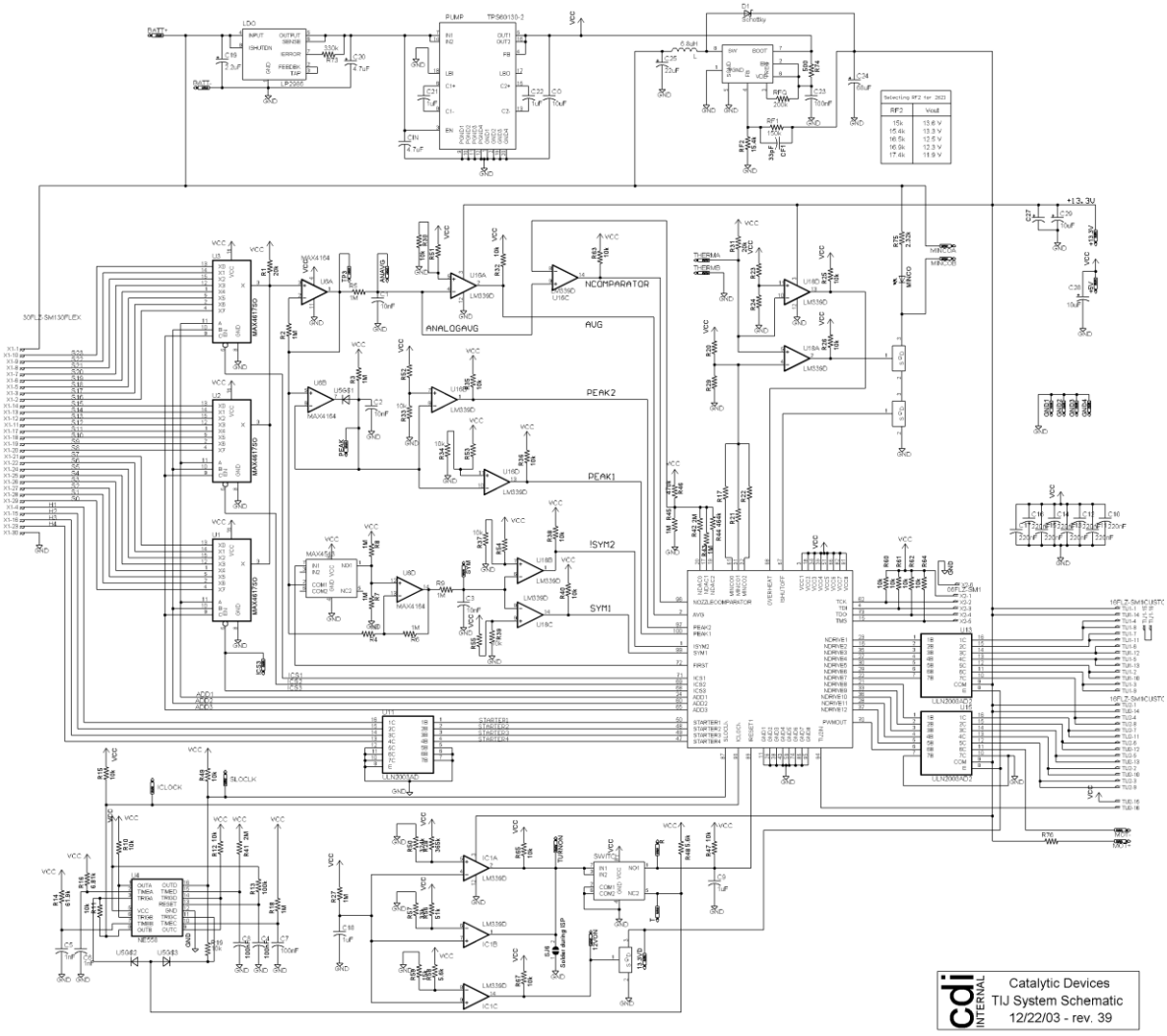

Figure 7. TIJ-Based AFCT Circuit Diagram

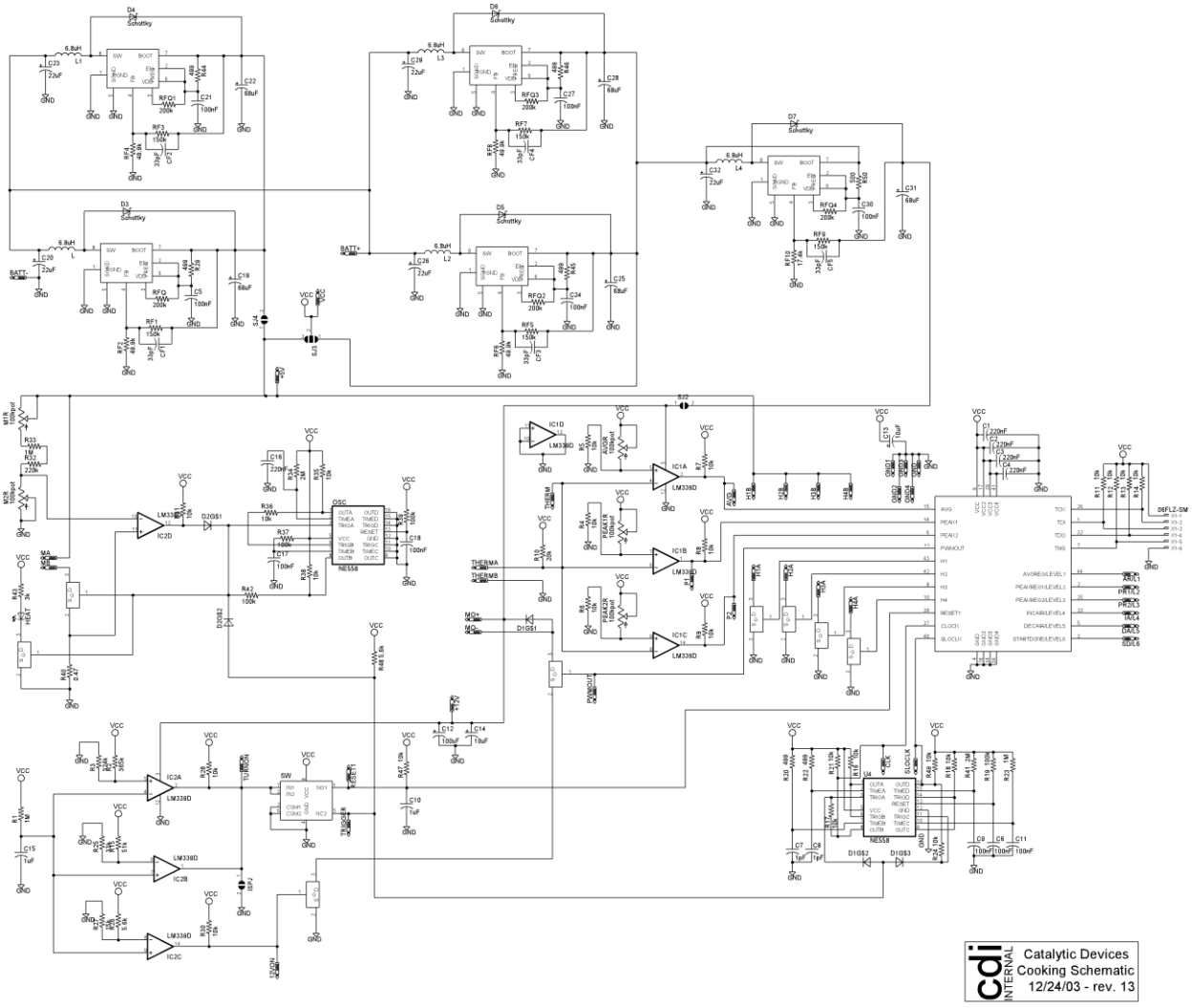

Figure 8. VEM-Based AFCT Circuit Diagram

2.2 Fuel Vaporization

Fuel vaporization and metering is a critical function for AFCT. Two widely different categories of vaporization are being developed at CDI to achieve the goals of the captive catalytic combustion applications being pursued.

The first method is the use of TIJ technology to meter the flow of microscopic quantities of fuel needed to achieve 100 watts of equivalent chemical power. The inkjet works by filling a small fluid reservoir with the fuel and applying a short pulse of electrical energy to a heater resistor located at the bottom of the well. This forms a rapidly growing vapor bubble that forces a portion of the liquid fuel above it to be ejected from the well.

The frequency of drop ejection is determined by how fast the well can be refilled and the amount of excess heat generated in the process. Too much heat will eventually cause the feed lines to the well to become blocked by an anomalous vapor bubble, similar to vapor-lock that can occur in older automobile carburetors on a very hot day.

It is therefore necessary to test each particular TIJ design to see how the drop size varies with firing conditions. **Figure 9** shows a graph of the TIJ behavior currently being used at CDI. It compares the firing frequency of the TIJ with drop size. The test is repeated over several TIJ units to see how a spread in manufacturing tolerances will affect performance.

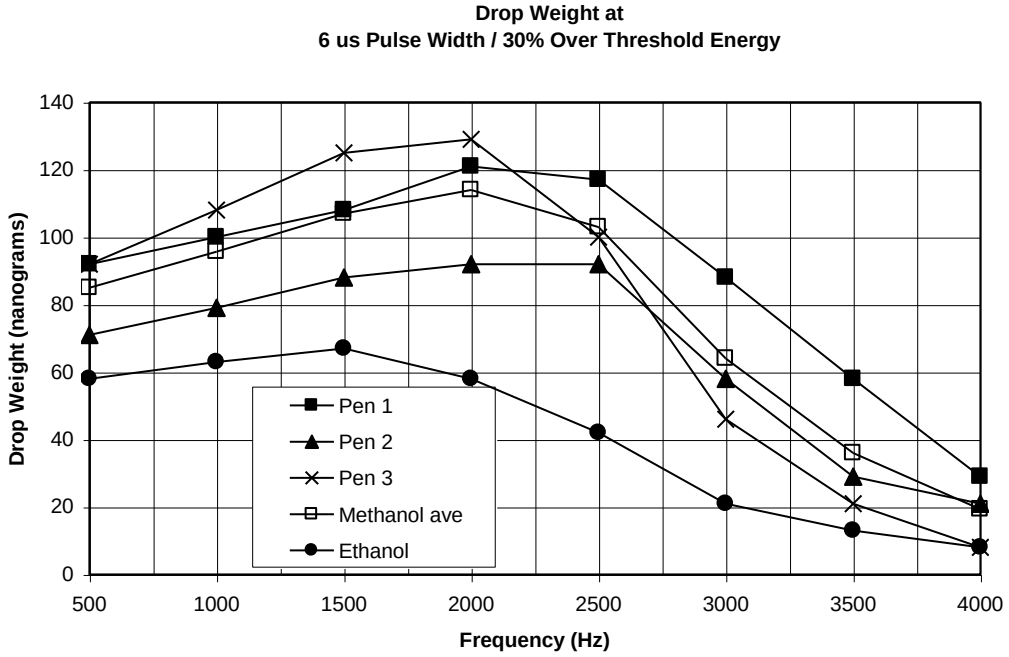

Figure 9. Natural Variation of Drop Size Between Randomly Selected TIJ Cartridges

The drop size being emitted from the TIJ is on the order of 75 microns in diameter. To complete the vaporization process it is necessary to add additional features to the TIJ fuel-metering system.

Figure 10 shows one method of completing the vaporization. The fuel cartridge is placed in a holding unit that supplies the control signals and power to the TIJ while directing the fuel droplets to a special receptor plate. The receptor is heated to complete the vaporization. The heat is supplied initially, for starting purposes only, by a miniature foil resistance heater and after starting by a micro-catalytic heater using a small portion of the main vapor stream.

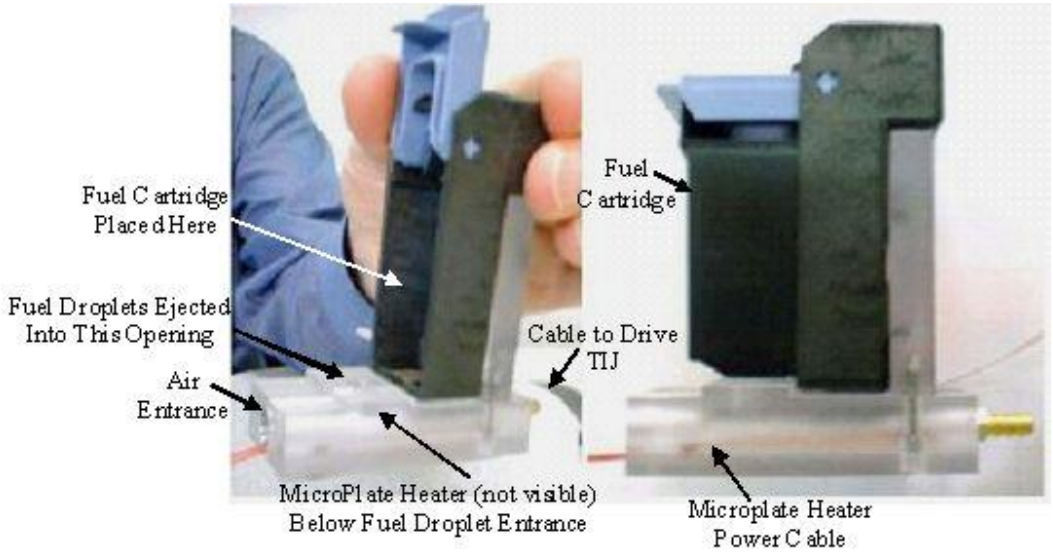

Figure 10. TIJ With Electric Microplate Heater

The efficiency of heat transfer to the droplets determines how much energy is required. A perfectly efficient transfer will use only the amount of energy as determined by the heat of vaporization. For methanol this would amount to about 5% of the chemical energy contained in a given mass of evaporated fuel. In **Figure 11**, a graph of the minimum power needed to vaporize the droplets, shows that the micro-plate heater uses 50% more energy than the theoretical heat of vaporization would predict. Significant improvements were obtained in the second phase effort.

Figure 12 illustrates an alternative TIJ vaporization scheme. In this diagram, the micro-plate is initially heated by electric power, as before; however, after a short period, the electric power is removed and the heat is supplied entirely by a catalytic reaction on the bottom of the micro-plate. The reaction is sustained by tapping a portion of the main vaporization stream and re-routing it to pass under the micro-plate where an exothermic reaction (flameless combustion) heats the plate.

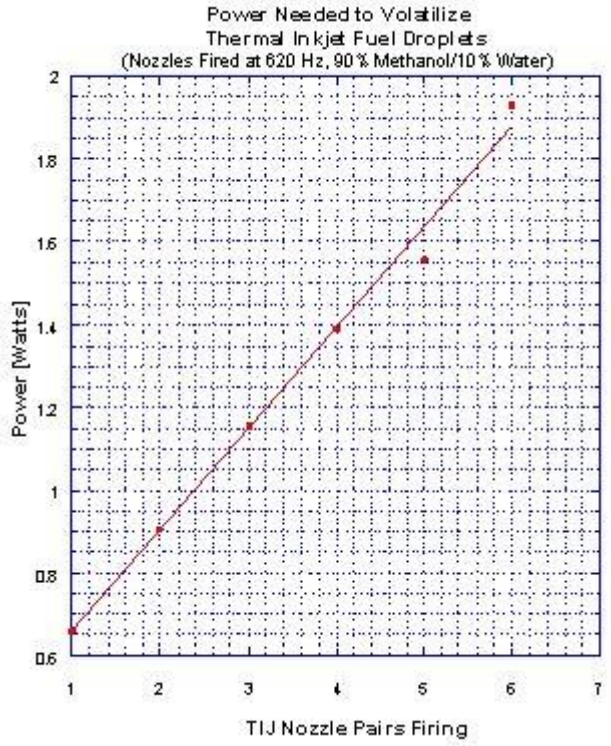

Figure 11. TIJ Electric Microplate Power vs Nozzle Pairs @ ½ Frequency

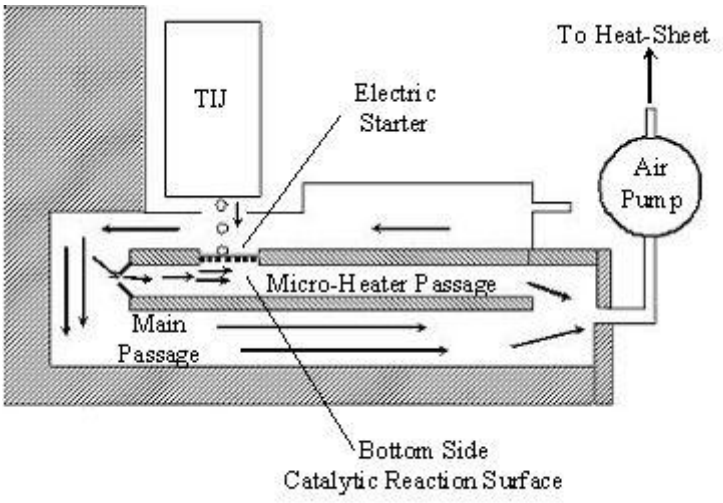

Figure 12. Conceptual Diagram of Catalytic Microplate

Figure 13 shows in greater detail the actual design for accomplishing the catalytic micro-plate heating. The unit consists of three separate layers. Each layer has a complex set of channels milled into the surface. When all three layers are coupled together, proper internal routing of the fuel/air stream occurs. The fraction of the main fuel/air stream that is tapped is determined by two set-screws located in the back of the unit.

Figure 14 and **Figure 15** show the new catalytically driven micro-plate vaporizer assembled with a TIJ cartridge inserted. In particular, Figure 15 shows the set-screws used to adjust the ratio of flow between the micro-plate catalyst channel and the main fuel/air flow stream.

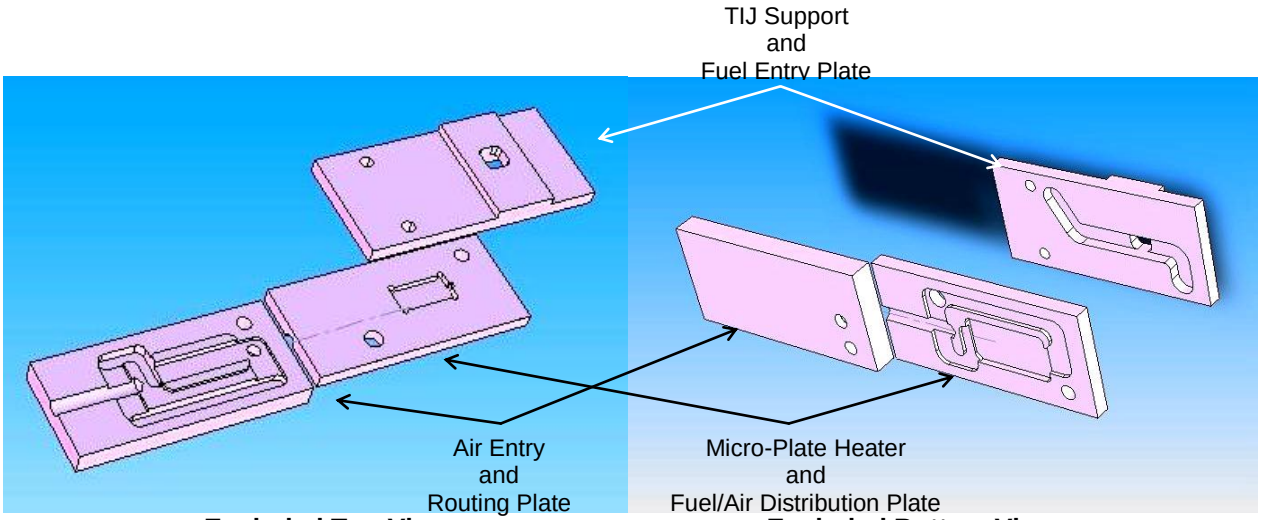

Figure 13. CAD Drawings of New Catalytically Driven TIJ Vaporizer

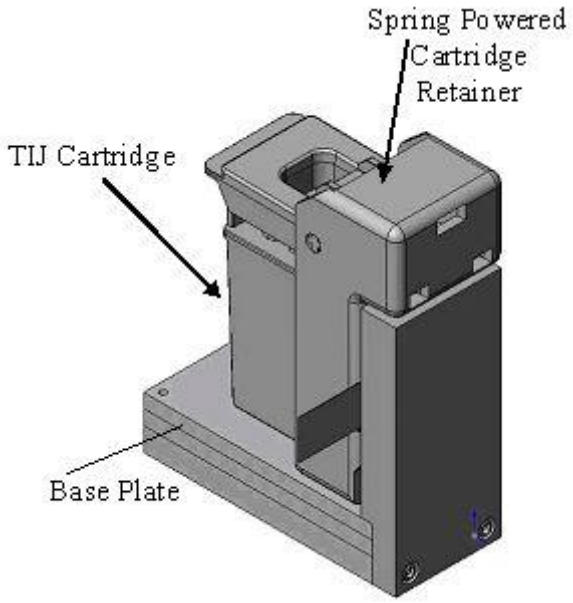

Figure 14. Single Head Catalytically Driven TIJ Vaporizer Body

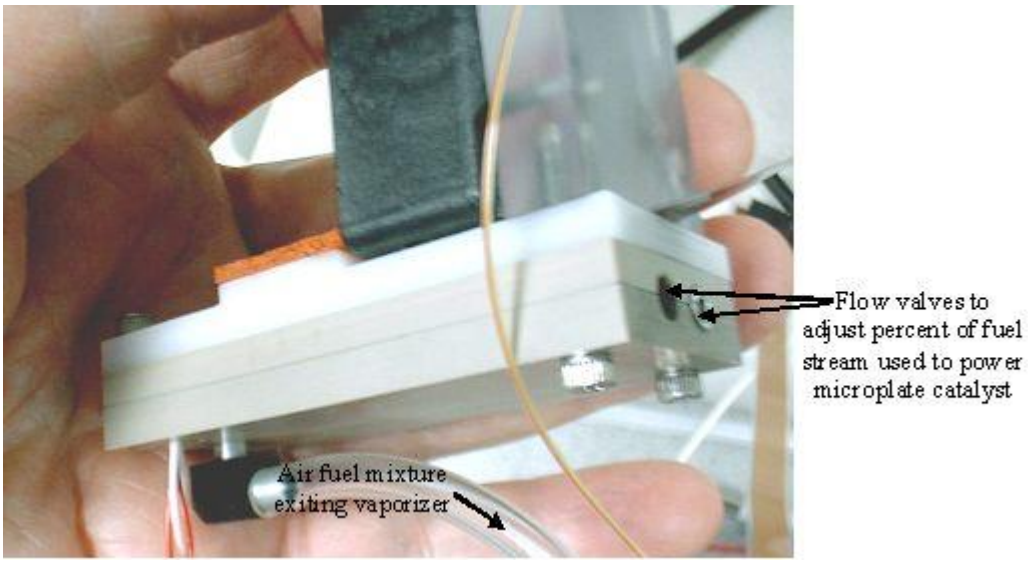

Figure 15. Assembled Single-Head Catalytically-Driven TIJ Vaporizer

On the bottom side of the micro-plate, a catalytically activated stainless steel foil is attached. The catalytic foil reacts with a portion of the main fuel/air stream that has been routed to flow to the bottom side of the micro-plate.

Nevertheless, it may still be necessary to improve the design of the catalytic micro-plate heater in order to efficiently vaporize 100 watts of chemically equivalent power; because, the vaporization rate is not just a function of the heat of vaporization, but also has a rate dependence that is not yet determined.

This rate dependence is partly determined by how effectively the heat is transferred to the alcohol droplets. If the efficiency is poor, the surface temperature of the micro-plate must continue to rise with increasing droplet rates. If the efficiency were perfect, the temperature would remain constant and only the power would be increased (i.e., rate of heat transfer to the droplets from the micro-plate).

Figure 16, **Figure 17** and **Figure 18** show the dual head option that is being planned to provide increased power capability. The microplate vaporization principle is the same as the single head versions shown above. One difference, however, is that these units are designed to allow automatic re-priming of the TIJ heads.

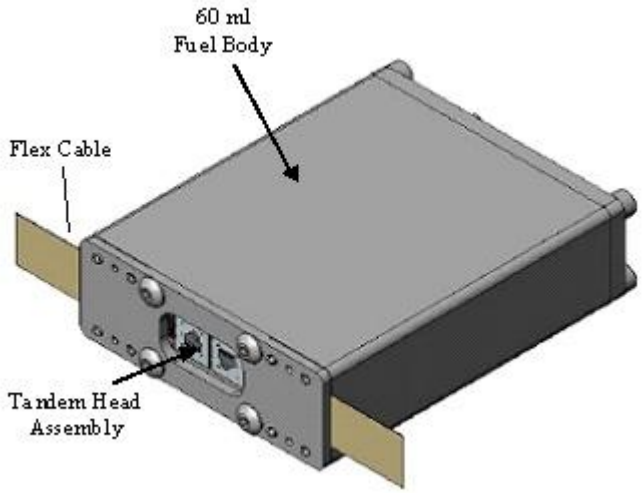

Figure 16. New Dual Head TIJ Design

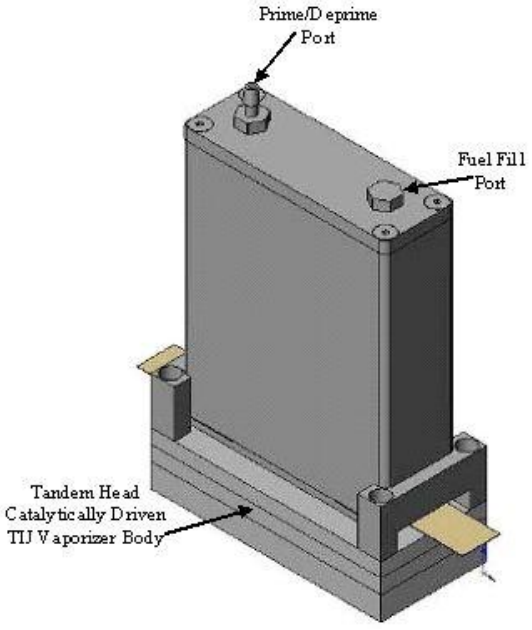

Figure 17. Dual Head TIJ Mounted

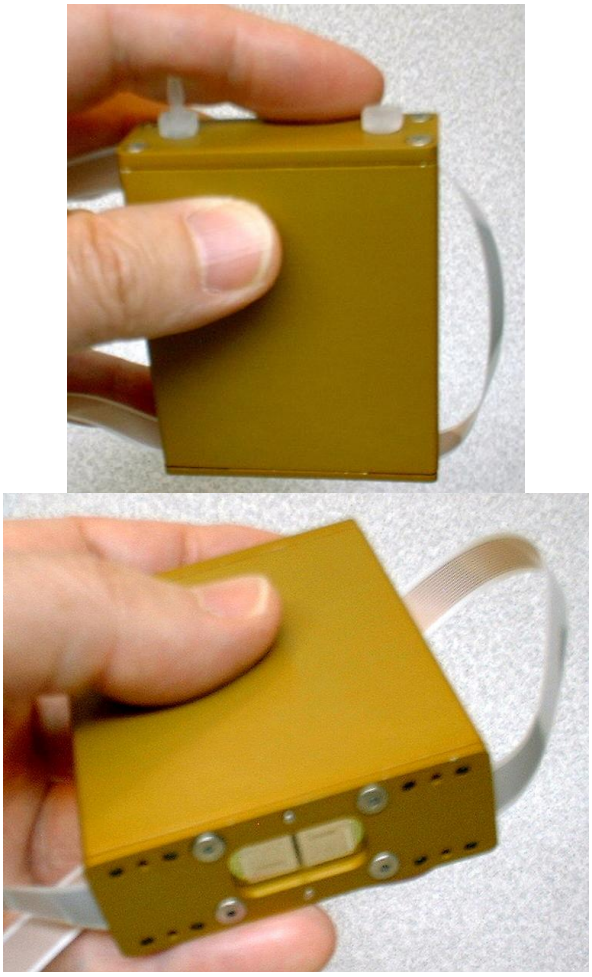

Figure 18. Assembled Dual-Head TIJ Design

An alternative and/or adjunct to the TIJ fuel-metering and vaporization approach is a scheme invented and patented by CDI. This method, known internally as the VEM technique, is a special subset of forced air evaporation methods. It has been advanced substantially over the first 12 months of this project.

It's principle of operation is based on extracting vapor from a pool of liquid fuel through the use of a special vapor extraction membrane. The membrane acts to prevent liquid fuel from penetrating the air flow cavity while allowing the vapor to be extracted across the boundary layer of the air stream near the membrane surface. The evaporation process "grabs" heat from the environment to satisfy the vaporization energy requirements. If left unchecked, the air temperature would drop to a point where evaporation would slow significantly. Thus, another source of heat is needed to keep the process running smoothly. The unique feature of the CDI technique is to provide the needed heat through the use a micro-catalytic reactor built into the evaporator unit.

Many different configurations and membrane structures have been examined. For instance, **Figure 19** shows a situation where the liquid fuel is placed within a hollow porous tube and the air stream is situated around the outside of the coiled fluid filled tube. The power output was not readily reproduced over time and control issues were raised that lead to it being abandoned for a more preferred design shown **Figure 20**.

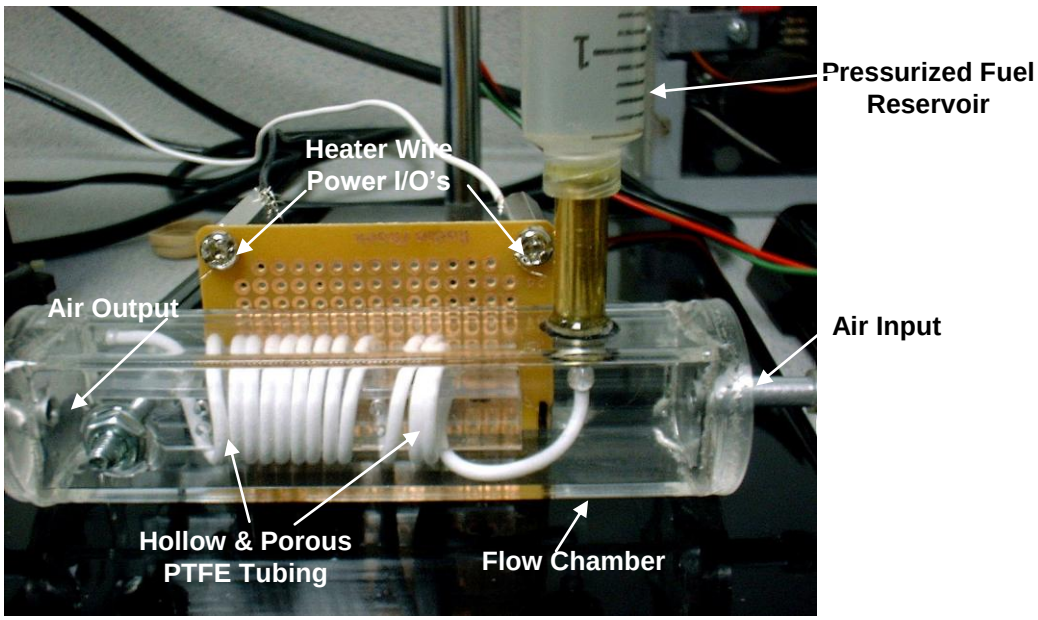

Figure 19. Test Set-up for Alternative Vaporization Scheme

Figure 20 shows the opposite approach to that shown in Figure 19, where the air stream is within a set of parallel hollow porous tubes and the liquid fuel is surrounding the tubes. This method has been found to be very successful in extracting fuel vapor at a consistent and predictable rate. It has no significant sensitivity to orientation and the energy (heat transfer) required for vaporization can be distributed over the whole volume of the fuel reservoir. This prevents the refrigeration effect from interfering with the vapor extraction rate.

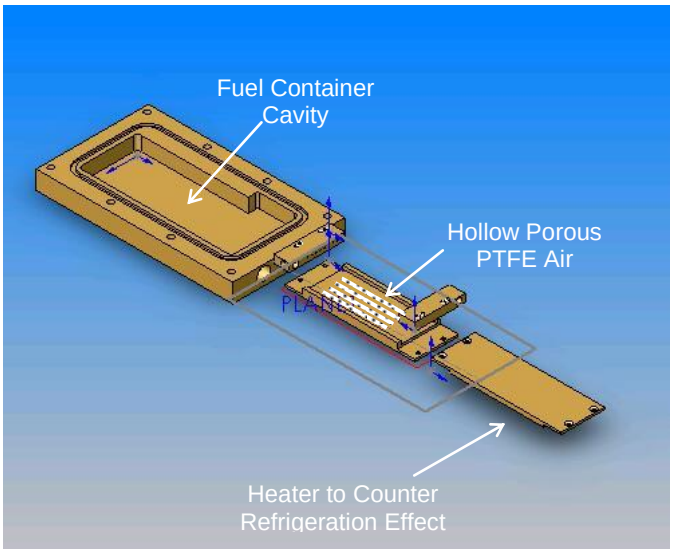

Figure 20. Version Two of Vapor Extraction Module (exploded view)

Figure 21 shows a similar version but with (a) a greater number of porous tubes and (b) increased length. This provides an increase in total surface area of tubes. By doing this, the total pressure drop is reduced and the heat transfer through the walls of the tubes is improved. Also seen in Figure 21 is the electric fuel warmer located just below the tubular membranes. This heater is only intended to retard the refrigeration effect until the fuel can receive energy from the flameless combustion elements, either by radiant or exhaust heat.

Figure 22 and **Figure 23** show one method of how the VEM unit could be reduced to practice for a particular application, i.e., heating a surface for cooking.

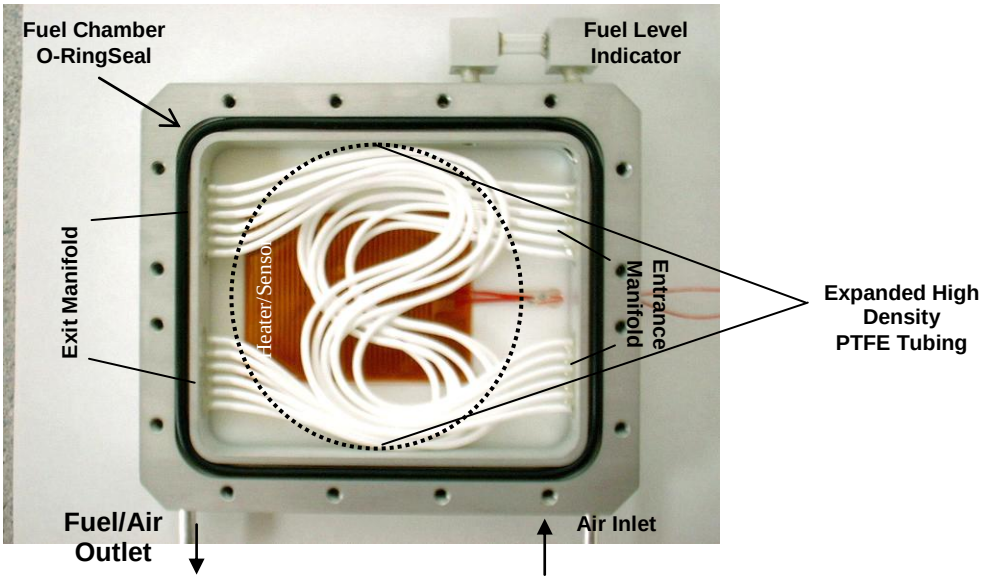

Figure 21. Vapor Extraction Membrane (VEM) Evaporator (top removed)

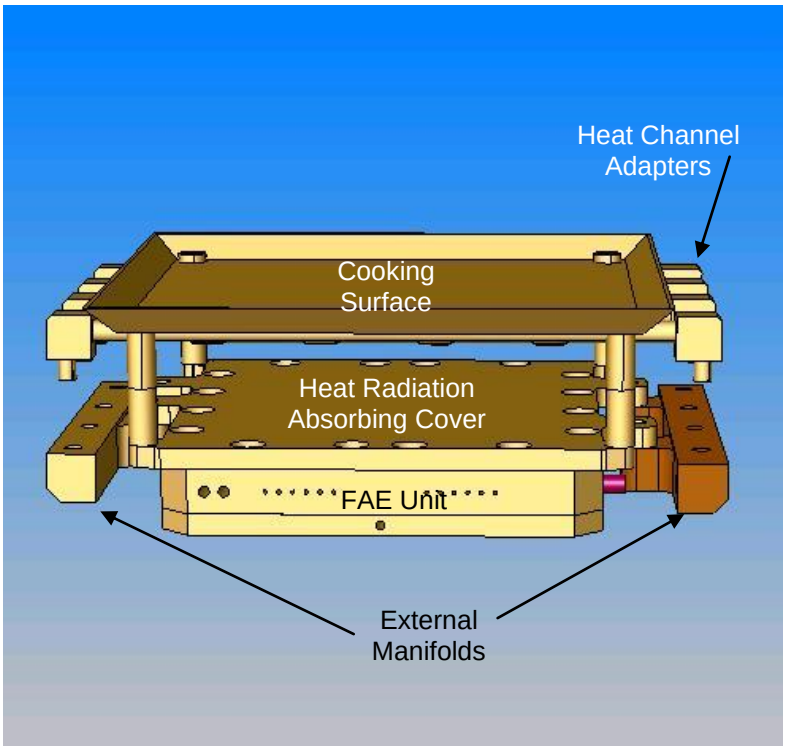

Figure 22. Radiant Heat Regenerative Feedback

Manifolds and adapters were added to reduce footprint by 50%.

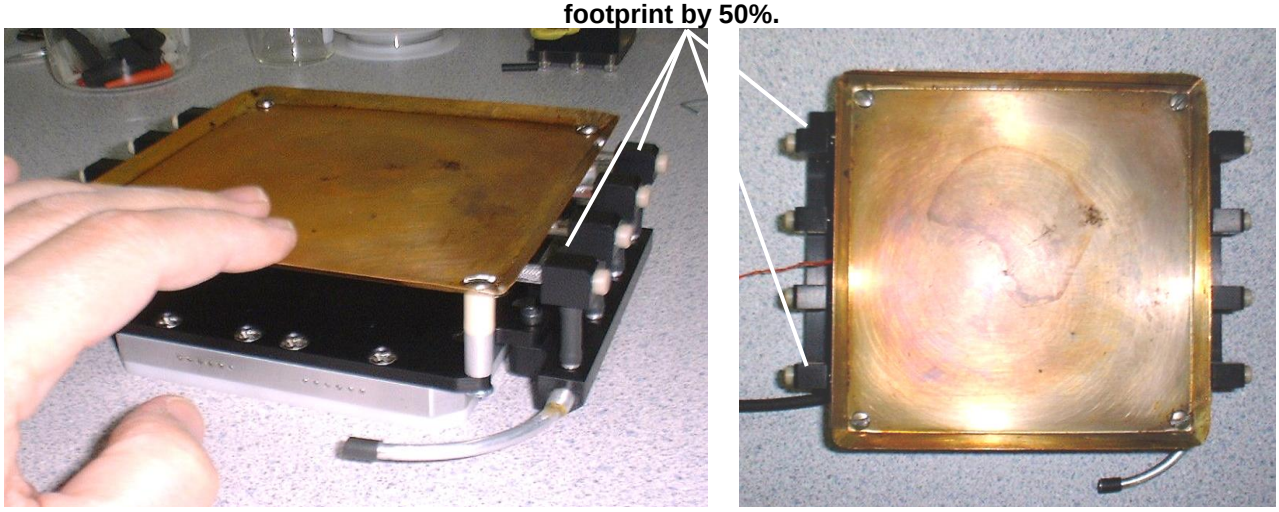

Side View **Top-View**

Figure 23. Partially Integrated 200-Watt Compact Catalytic Cooker

Figure 24 and **Figure 25** show the electronics, air-pump and scrubber used with the "partially" integrated catalytic cooker that was shown in Figure 23.

Figure 24. Scrubber, Blower & Electronics

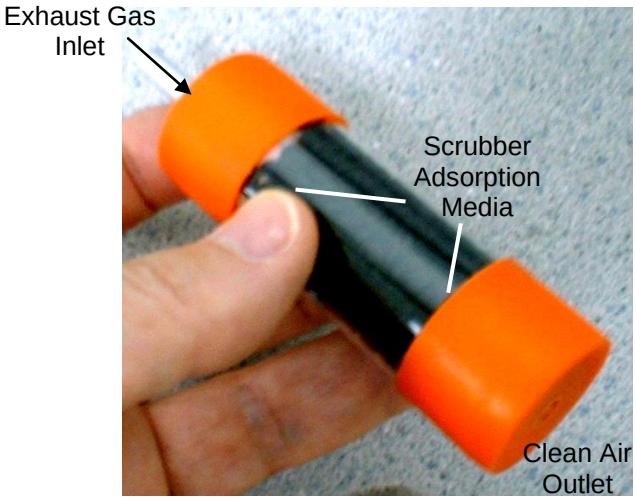

Figure 25. Scrubber Detail

Figure 26 shows a graph of the performance data for the VEM unit shown in Figure 23. It compares the fuel extraction rate, as measured in watts of equivalent chemical power, to various conditions of operation.

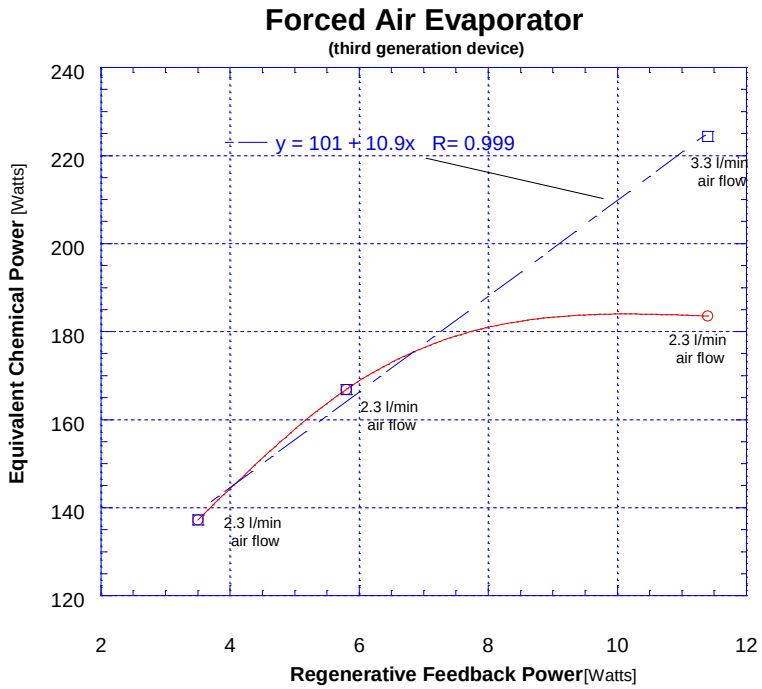

Figure 26. Fuel Extraction Rates for Different Conditions

It is apparent from the graph that for a given air flow rate, for example 2.3 liters/min, an increase in heat transfer to the fuel reservoir will increase the extraction rate. This will continue until the flow stream vapor concentration reaches the methanol vapor saturation level.

At this point the air stream becomes supersaturated and begins to condense out of the stream. This is demonstrated by the red curve in Figure 26. By increasing the air flow rate (e.g., 3.3 liter/min) the extraction rate moves, once again, into the linear portion of the curve. This demonstrates that as long as the air flow rate is properly matched to the heat transfer, a predictable power output is obtained.

Figure 27 and **Figure 28** show the third generation enhanced VEM. It differs from the version shown in Figure 21 by integration of the electronics, scrubber and air pump into one autonomous unit. It also differs by having internal geometric modifications that enhance heat transfer from the exhaust stream to the fuel reservoir. In addition, the number of tubular membranes and there placement within the reservoir cavity enhance coupling of the electric fuel heater (used only during start-up) to the membrane surfaces.

It is believed the unit shown in Figure 28 can be made smaller, lighter and cheaper, while being able to produce 300 to 400 watts output (1025-1370 BTU/hour).

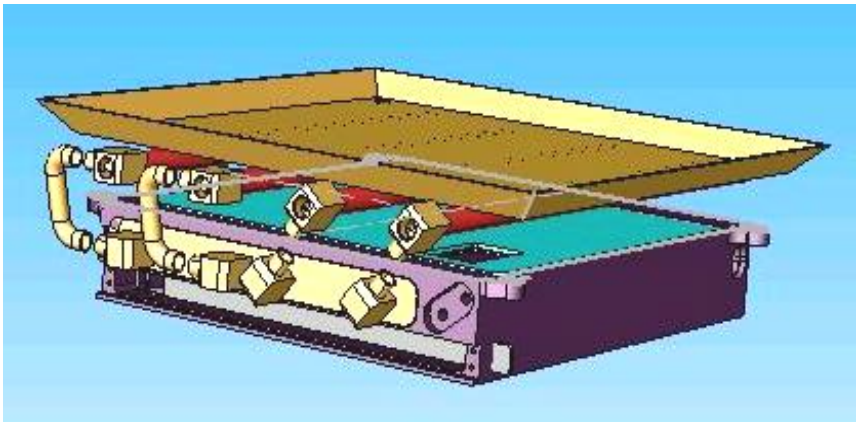

Figure 27. Completely Integrated 300-Watt Flameless Cooker

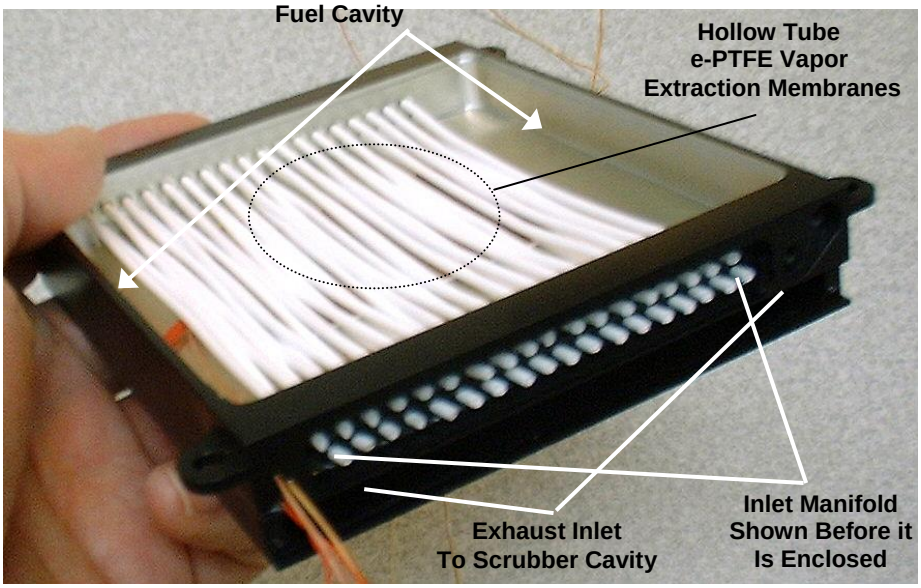

Figure 28. Partial Assembly of New Forced Air Evaporator

Something else to note in Figure 28 is the tubular geometry of the vapor extraction membranes. One advantage is that the surface area of the membrane is quite large compared to the space that it occupies. The main disadvantages, are that they are expensive to produce and labor intensive to install. Both these drawbacks can be overcome by switching to ribbon-like or sheet-like membrane geometry. In phase 2, CDI will be comparing the two geometries in terms of effectiveness, cost and ease of assembly. The flat sheet-like shape of the ribbon membrane also lends itself to certain standard assembly techniques desirable in mass production.

It should be pointed out that this type of fuel metering and vaporization technology is restricted to fuels that have certain properties, in particular saturation pressures and molar heat contents that are within the right range. For instance, ethanol is a suitable choice, even though its vapor pressure is substantially less than methanol at the same temperature; because, it is compensated by its increased heat energy per unit saturated volume of air and produces roughly the same chemical energy output under similar conditions. A number of other liquid fuels, such as gasoline, and its derivatives such as hexane, heptane, and octane, also meet these requirements. Heavier fuels, such as JP-8 and diesel may best be suited for the TIJ or other mechanical approach to breaking the fluid into droplets such as ultrasonic nebulization.

Some advantages to ethanol are that its energy per unit liquid volume is greater than methanol and it is relatively non-toxic.

Ultimately, CDI believes production cost of the whole VEM vaporization unit can be reduced to less than 10 dollars, including air pump and electronics. Costing for the TIJ approach is not yet known.

2.3 Air Delivery System

Figure 29 illustrates the internal mechanical structure of the rotary-vane air pump design chosen. The requirement was for a device that can operate at high efficiency under a backpressure of several inches of water, provide flow rates from zero to 4 liter/min on demand, have small physical size, be relatively quiet, and manufacturable at low cost.

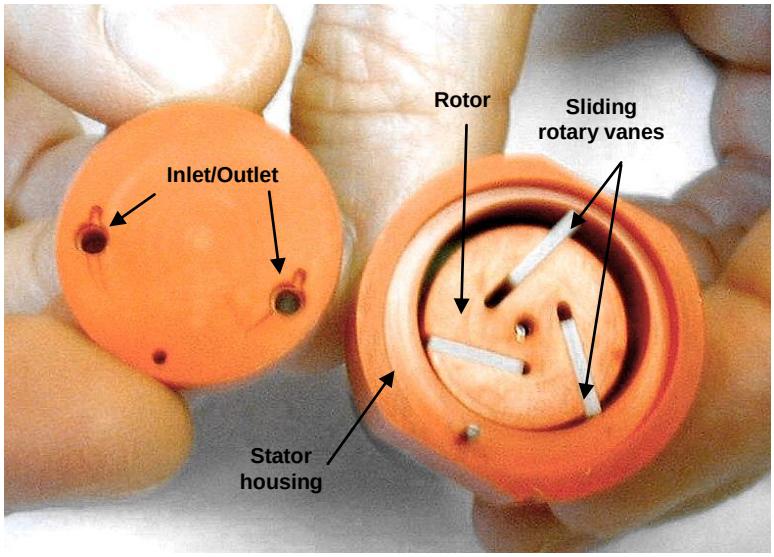

Figure 29. First Prototype of New Air Pump Design

Because the whole system is portable and battery operated, efficiency plays a significant role in making the application practical. **Figure 30** shows a graph of the power requirements versus air flow rate for several off-the-shelf air pumps of similar design to that shown in Figure 29.

Choice of materials, number of vanes, chamber geometry parameters (e.g., eccentricity, rotor diameter to thickness ratio, etc.) and drive mechanism (i.e., electric motor type) determine the overall performance of the pump. Often the trade-off is between backpressure capability and flow rate. For AFCT applications, backpressure has been minimized to allow access to the higher flow rates and improve overall system efficiency.

Figure 31 illustrates the linear relationship between flow rate and backpressure. This is typical of all rotary-vane air pumps. **Figure 32** demonstrates a typical air-pump efficiency relationship versus flow rate and motor drive voltage. The graph displays efficiencies in terms of work done on the fluid (e.g., air) divided by the work done by the motor. It is interesting to note that only about 20% to 23% of the motor energy is being converted into movement of the air.

It is clear from this figure that the higher operating voltage provides a wider range of high efficiency operation than the lower voltages. This is one reason why the use of motor speed control schemes, where the motor voltage is held constant while the on-time is controlled are preferred (e.g., pulse width modulation) and is used by CDI. In this way overall system efficiency is improved. Another reason is of course that the controlling electronics work most efficiently under a pulsed power control scheme (e.g., pulse width or frequency modulation, etc.).

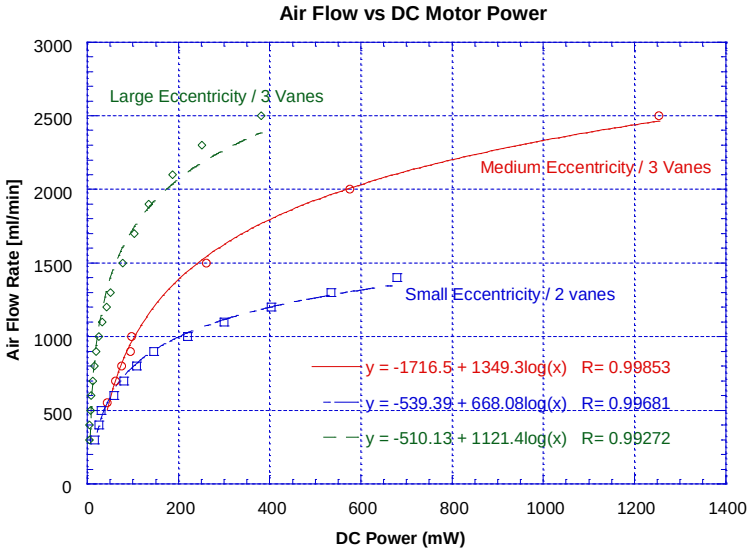

Figure 30. Flow Rate vs. Power Consumption

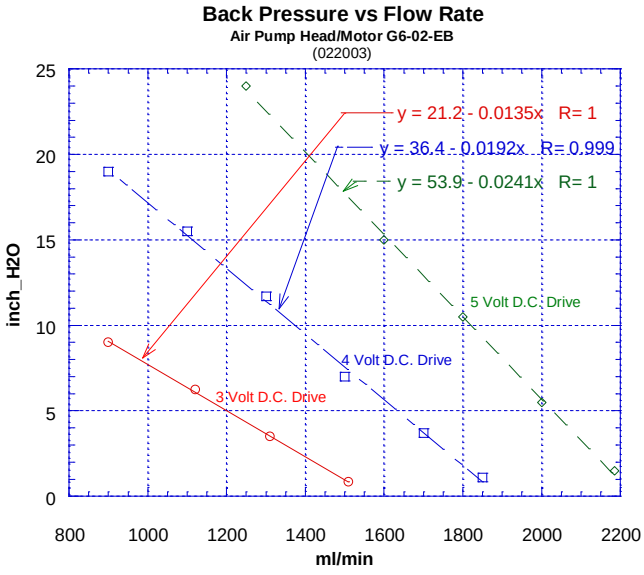

Figure 31. Air Pump Back Pressure vs. Flow Rate

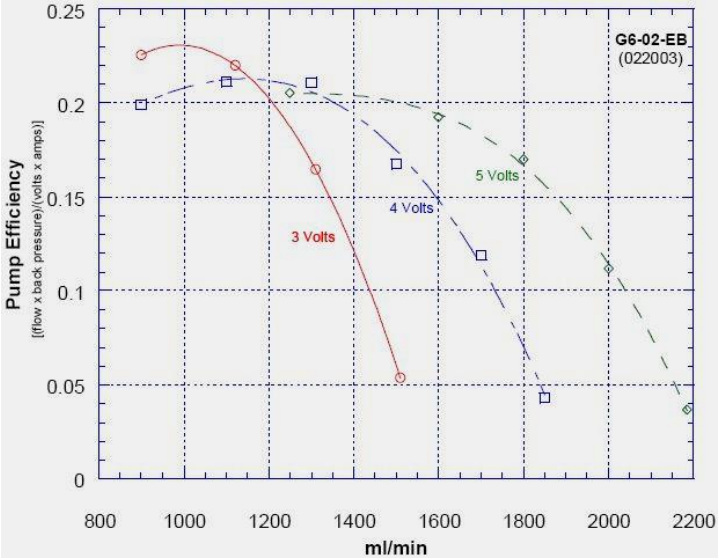

Figure 32. Air Pump Efficiency vs. Flow Rate

The choice of fuel vaporization strongly influences the choice of air-pump design. **Figure 33** is a photo of the latest high efficiency, high flow-rate rotary-vane air pump manufactured and designed by CDI. Its physical size can be reduced further (e.g., 20%) without reducing its performance and will be done at a later time.

It was designed to take advantage of the VEM scheme for fuel vaporization invented at CDI. Because the VEM method can produce high equivalent chemical power outputs (e.g., 300 watts), the airflow rates must be larger than the TIJ fuel metering and vaporization method, which in dual TIJ head format will put out a maximum of 100 watts.

It should be pointed out that from a technical perspective, the general TIJ technique has not been the source of the limited power but rather the effects of trying to use the lowest cost TIJ option. Higher power capability does already exist in other more expensive TIJ based technologies at Hewlett Packard. However, they do not fit into the business-model/cost-constraints thought to be necessary to penetrate numerous market niches and are therefore not being pursued at this time.

Figure 34 illustrates the flow rate versus power consumption of the CDI air-pump. The graph shows that this unit readily meets the system requirement of achieving 4 liters/minute of air flow utilizing less than ½ watt of electrical power. These values are for 1 inch of water backpressure.

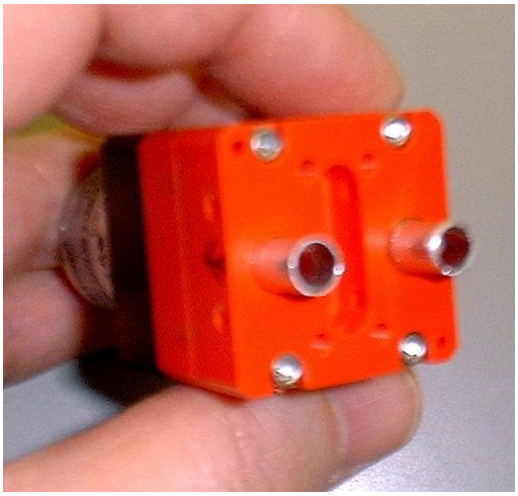

Figure 33. CDI's High-Flow Rotary Vane Air Pump

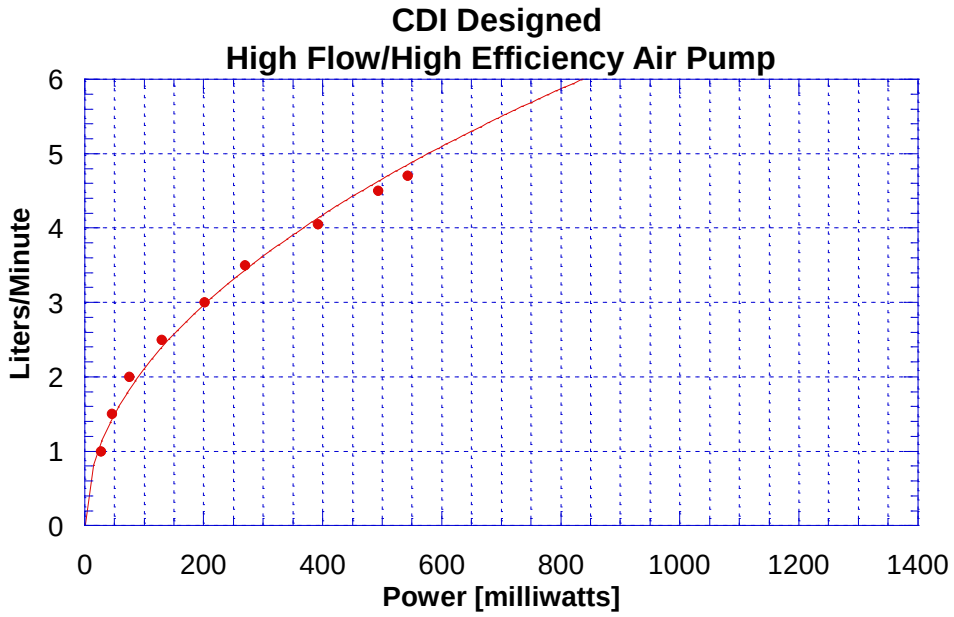

Figure 34. Air-pump Performance Curves
(1 inch of water backpressure)

Figure 35 and **Figure 36** are the raw data from which Figure 34 was derived. Note that the current requirements are minimal across the whole range of operation.

This is important, since portable designs place a heavy burden on the battery capability. A simple calculation of battery life based on amp-hour capacity is seldom reflective of the actual battery life except at very low current draw. The lower the overall current draw, the longer the batteries last and the closer that their predicted life approaches the simple amp-hour calculation. High currents and/or pulsed current operation substantially complicate the predicted life of a given battery for any real application.

Figure 35 shows that in order to obtain the higher flow rates using that particular air pump, the battery voltage will need to be maintained above 3 volts. Since most primary batteries are either at or below this level, the use of a DC/DC boost convertor or multiple batteries will be required.

From **Figure 36** it can be determined that a relatively small and inexpensive boost convertor design is sufficient since the current requirements are minimal. Transient, high current demands,

such as the impulse resistance starters (e.g. 0.75 amps) can be driven directly from the battery(s) to avoid stressing the boost convertor. This simplifies the power supply and maximizes battery life.

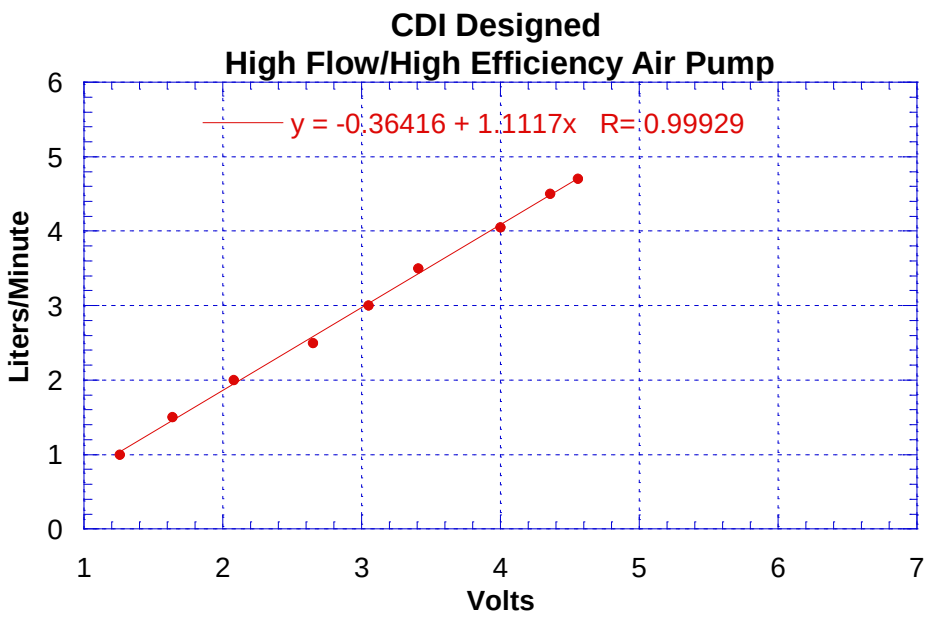

Figure 35. Air-pump Flow Rate vs. Voltage

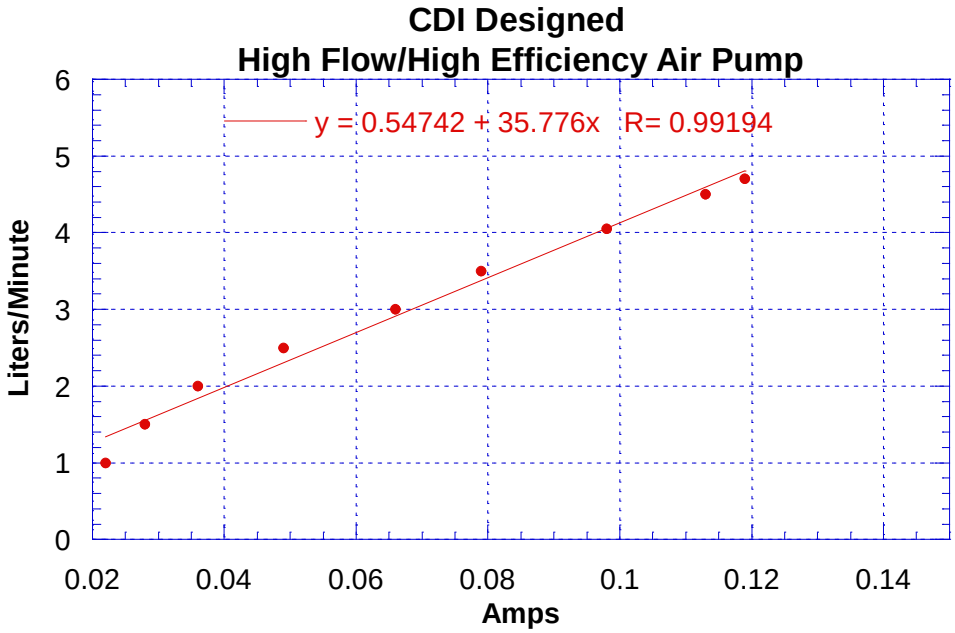

Figure 36. Air-pump Flow Rate vs. Current

2.4 Catalytic Heat Element Fabrication and Design

The catalytic heat element is at the heart of AFCT. During phase one, CDI explored a variety of ways to construct these elements in order to enhance their operation for each application.

Figure 37 illustrates the morphology of a typical heat element. Selection of the materials that make up the component parts of the heat element comprises the majority of the optimization process. Modeling the physical behavior of the combustion process as a function of both the heat element geometry and its relation to the feed channels, represent the remainder of the optimization.

During phase one CDI was able to determine, based on theoretical constructs, that improvements to the heat element performance is possible. These were scheduled for fabricated in phase 2. In particular, it was determined through modeling that new methods of fabrication, along with alternative feed geometries and new channel combustion dynamics, will lead to greater repeatability between elements. These advanced prototypes were developed in phase 2 as discussed in section 4.0.

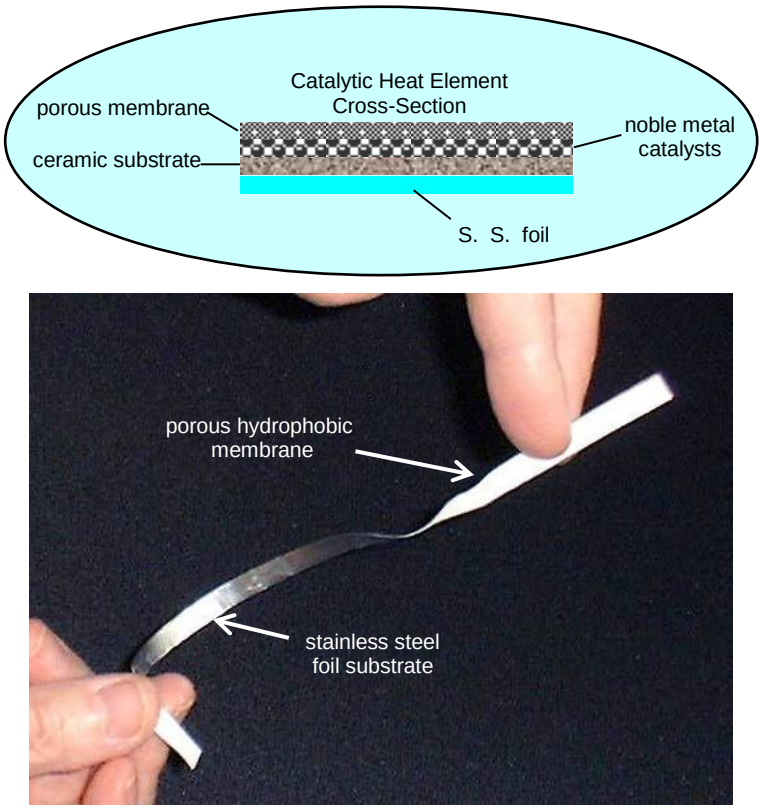

Figure 37. Typical Heat Element Structure

Figure 38 shows a version of a flexible heat-sheet sized to fit into an MRE food pack and incorporating a symmetrical feed-channel geometry. The heat elements are attached to the polyimide mid-sheet on the side opposite the thermistors shown. It consists of a composite lamination of several layers. The bottom layer is shown in **Figure 39**. It contains the flow channels that direct the fuel/air mixture to the catalytic heat elements. After laminating the polyimide mid-sheet to the bottom layer, the heat elements become the interior roof of the flow channel.

In this way, the fuel/air mixture flows over the heat element and reacts with the catalyst, producing heat. The choice of materials for all the layers is of critical importance. The bottom layer is made out of a closed cell polymer foam (ECH) capable of withstanding relatively high temperatures (350°F) and compatible with the catalyst.

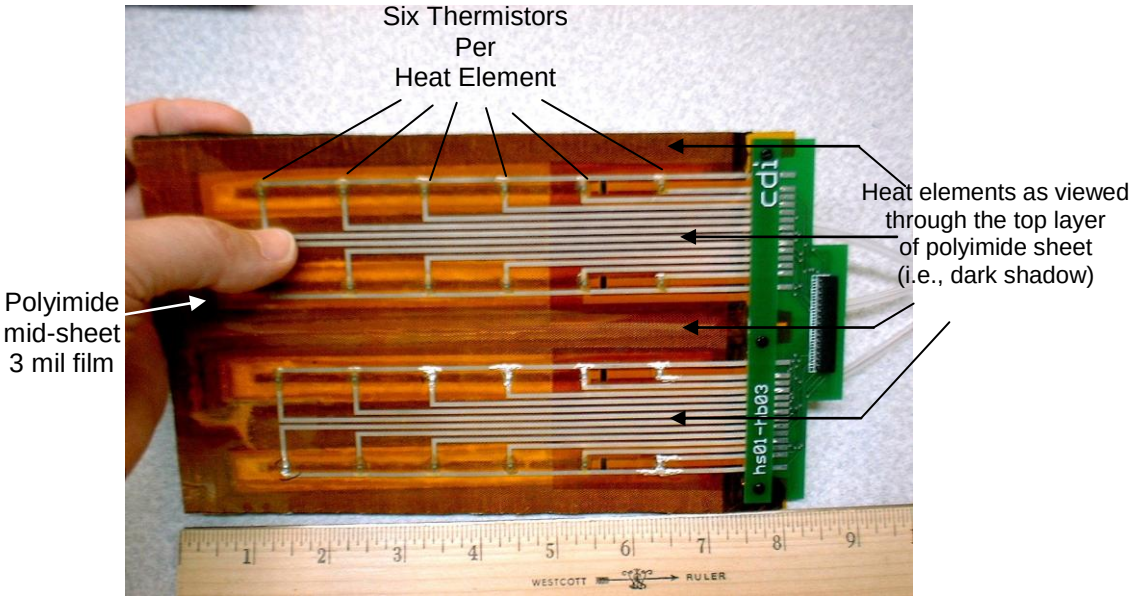

Figure 38. Four Channel Flexible Heat Sheet

To spread the heat quickly, an expanded metal foil is bonded to the bottom of the mid-sheet before it is laminated to the bottom sheet. A third layer (not shown) may be bonded to the top of the mid-sheet depending on application, need to further spread the heat, and the level of protection deemed necessary for the sensing grid.

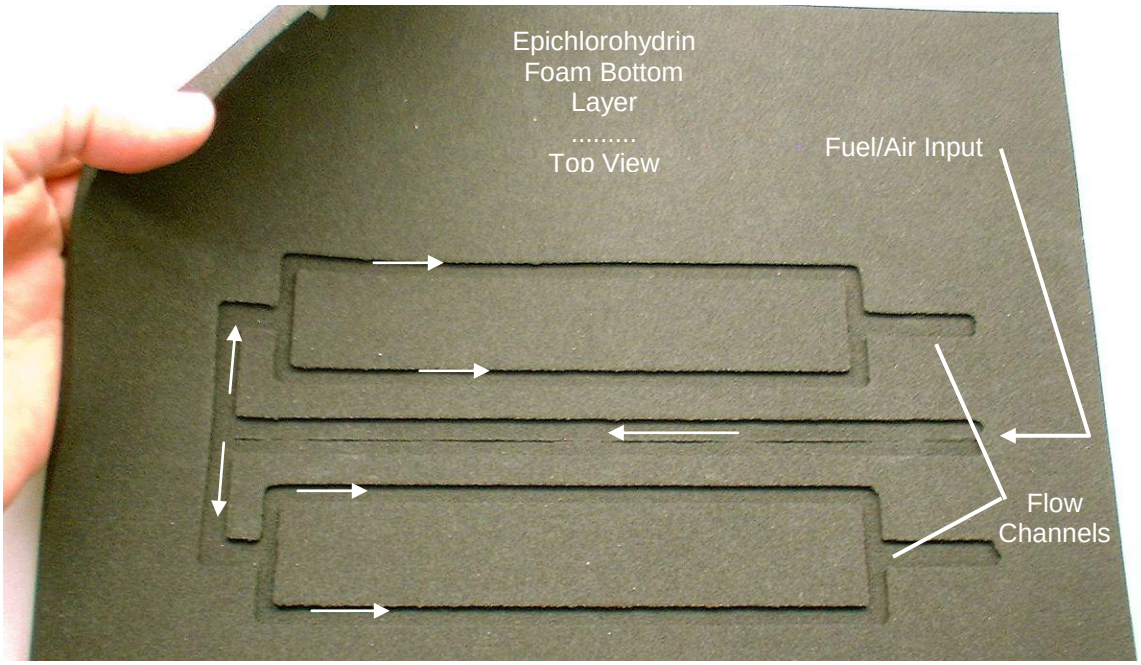

Figure 39. Top View of Foam Bottom Layer Before Lamination to Mid-Sheet

2.5 Supporting Technical Efforts

Figure 40 shows how each catalytic heat element is tested to determine some of its combustion properties. The two properties of great interest after fabricating the elements are (1) overall catalytic activity, and (2) uniformity of the reaction across the heat element.

The elements are placed in the flow channels as shown in the right hand photo of Figure 40. The flow channels are then sealed with a lid or top plate. A fuel/air mixture is metered into the channels at selected equivalence ratios and flow rates.

As the exothermic catalytic reaction proceeds, temperature sensors shown in the left hand photo of Figure 40 send information to a computerized data logging system.

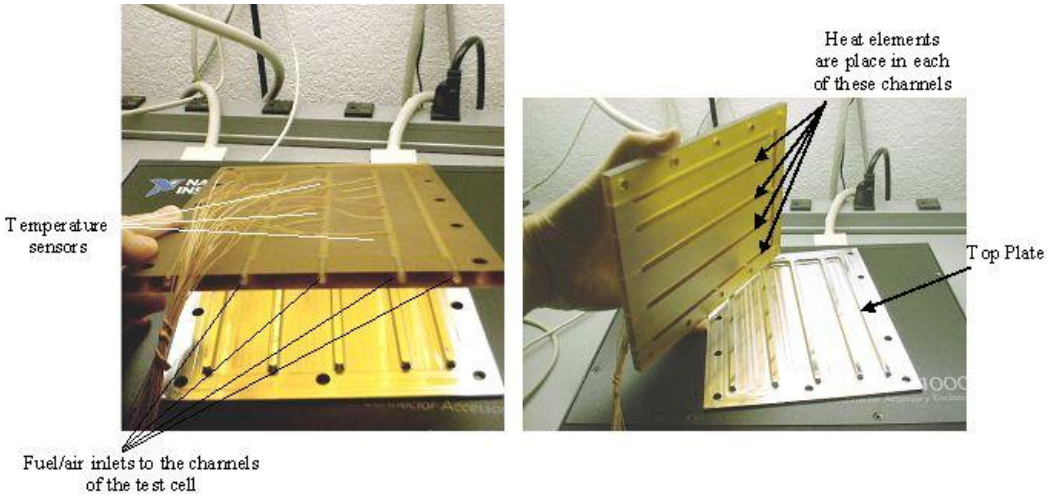

Figure 40. Heat Element Test Cell

The real-time spatial temperature profiles are then displayed on a computer screen using a LabView virtual instrument program developed at CDI. **Figure 41** shows a typical temperature profile display using the LabView program. Each of the four channels is displayed here as a set of bars (six bars per channel). The height of each bar represents the temperature at the exact point where each thermocouple sensor touches the backside of the heat element foil.

Each channel contains one heat element with six temperature sensors placed uniformly along the six-inch long channel and in direct contact with the heat elements. Since the elements are fabricated on 0.001"-thick stainless-steel foil, the bottom temperature is a close representation of the top (reactive) surface of the element.

Figure 41 shows a typical case where the highest temperature for each channel occurs near the entrance to the channel. This is identified as the typical "collapsed state" of combustion and is the antithesis of the desired state where combustion is uniform along the whole length of the element. This information is then used to determine how best to properly allocate the catalyst concentration along the length of the element, to result in a uniform temperature profile.

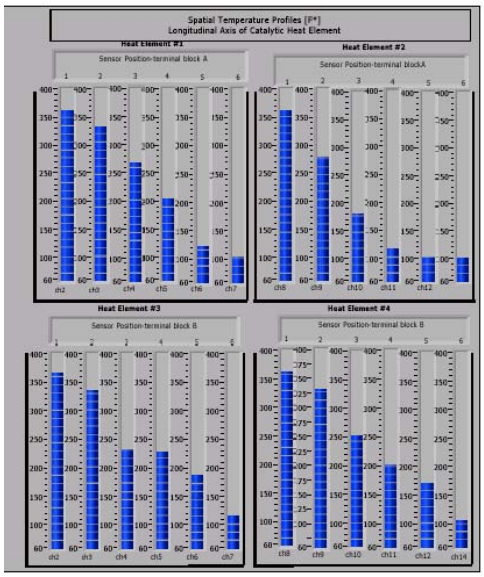

Figure 41. Virtual Instrument Temperature Display

Figure 42 is a photo showing mid-sheet prototype that has the temperature sensors silk screened onto its surface. It differs from the older mid-sheet design in two ways. The conductive traces are etched copper (instead of screened-on conductive traces) and the thermistors are screen printed using a specially formulated compound by Ormet Circuits. The intent was to replace the expensive and low-reliability surface mount thermistors with a low cost, robust screen printed structure.

The new thermistor formulation was tested by placing the mid-sheet in a temperature-controlled press and the temperature was varied from a room value of 25°C to 200°C (77-390°F). The voltage across each thermistor was read and recorded as the temperature of the sheet was changed. **Figure 43** provides a graphical representation of the screened-on thermistor resistance values (read as a sensed voltage) presented as an average (all twenty-four thermistors), peak outlier and lowest value outlier for each temperature.

From this data it was determined that the wide variance in thermistor values rendered the thermistors un-usable for the intended purposes. In addition, it was concluded that the thermistors tended to vary noticeably overtime, presumably due to absorption of humidity. While it might be possible to eventually formulate a stable compound, it was felt this would require an effort greater than Ormet Circuits management was prepared or willing to tackle.

An alternative approach another approach was attempted that takes advantage of the reel-to-reel plastic film metalization technology that is now available. This was combined with the reel-to-reel photo etching machine technology. The essential method being that a polyimide film is coated with a thin layer (<1 micron) of nickel or iron/nickel and then patterned in a serpentine structure.

The high TCR positive temperature coefficient of the metal provided a predictable and measurable increase in resistance as the temperature increases. The final step is to send it to a high-volume screen printing service bureau to deposit the necessary conducting paths that connect everything together.

Although the results looked promising, the effort was exceeding the planned funding level and was terminated before a definitive study could be completed. Nevertheless, this approach appears to have the greatest potential for high volume production and low cost.

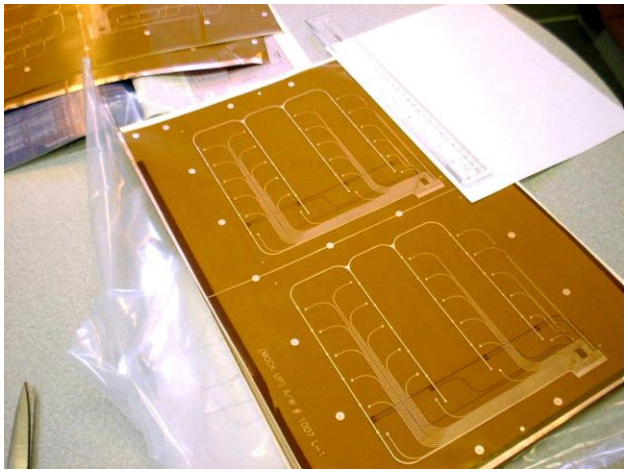

Figure 42. Photo of New Mid-Sheet Flex Circuit Design

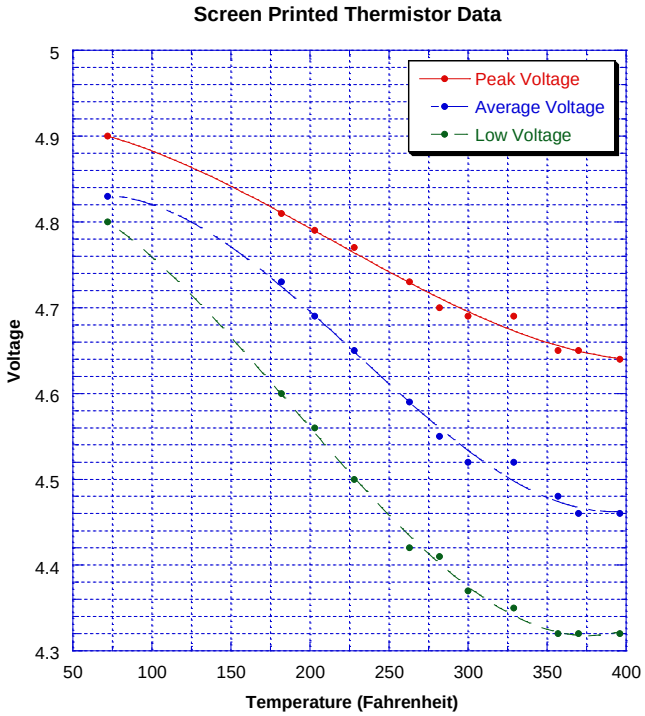

Figure 43. Screened-On Thermistor Performance

Another supporting technology important to development of AFCT is in manufacturing: precise control of catalyst deposition onto the heat element substrates. One concept that appears very promising is to utilize the natural metering properties of the TIJ technology to deposit these fluids onto the ceramic-coated surface of metal foil.

The TIJ nozzle position can be controlled using standard plotter driver software. The amount of deposited material can be controlled using half-toning techniques already developed for printing high quality images. The key to good results is to calibrate the already existing software routines with actual quantitative measurements of amounts deposited and determine heat element performance using the test cell shown in Figure 40.

Figure 44 shows the result of a test with a colloidally-suspended platinum solution prepared at CDI. The half-tone pattern shown was selected by engineers at HP to emulate a controlled deposition. This pattern and similar variations were then applied to a number of ceramic coated foils.

In practice, the goal is to impart a graded concentration of catalyst to the heat element substrate. In theory this should allow for very repeatable heat element characteristics among a large group of manufactured heat sheets. This is a prerequisite to cost effective manufacture.

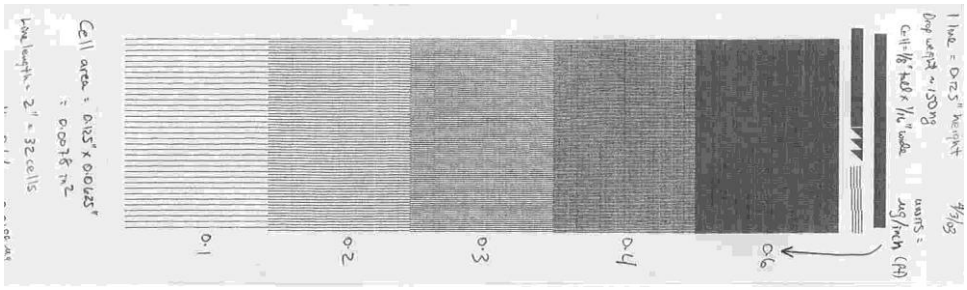

Figure 44. Catalyst Deposition by Thermal Inkjet Method

3. Phase 2 Development Activities

Phase 2 development activities are directed chiefly toward (a) finalizing the system design , (b) determining "best of breed" in the subsystem elements and (c) testing and comparing complete prototype systems.

Subsystem elements refers to elements like (a) the vaporization and fuel/air delivery subsystem (b) catalytic heat sheet (i.e. reactor) subsystem, and (c) electronic control subsystem. Each subsystem can be implemented in more than one way using different types of core technologies to achieve a similar functionality.

The remaining portion of this report details the technical efforts expended to explore the alternative approaches to each subsystem and then perform the trade-off study necessary to arrive at the best solution.

3.1 Alternative Vaporization & Metering Techniques

Each of the vaporization and fuel metering approaches discussed in this and previous sections operates in the VEM mode rather than the passive diffusive membrane evaporation mode originated by CDI and explained in CDI's earlier patents. The VEM mode was chosen because of its relative ease in meeting safety requirements and its precise power control capability.

Perhaps the most essential element of any catalytic combustion process is the proper delivery of an appropriate quantity of fuel and air to the catalytic surface. The choice of method in vaporizing the fuel and mixing it with air will dramatically impact the choices in the rest of the system.

For instance, the use of a TIJ-based vaporization process will substantially increase the complexity of the controlling electronics, as well as affect broader concerns like fuel supply approach (e.g., replaceable cartridge or refill approach), orientation sensitivity, ability to scale to larger power outputs and manufacturability (e.g., costs, supplier issues, safety, etc.). This must be weighed against the TIJ benefit of having precise control over the fuel metering process.

Each vaporization technique presented below has similar trade-offs that will need to be made in order to assess the best choice for a particular application.

3.1.1 Vapor Extraction Membrane Evaporator

CDI has invented several alternatives to the TIJ vaporization approach. A particular method, a subclass of the forced air evaporation category (FAE), known as vapor extraction membrane elaborated on in this section.

Figure 45 below shows a completely assembled 3rd-generation VEM attached to a water container designed to boil water. This VEM-based system, unlike the one shown earlier in Figure 21, Figure 22 and Figure 23, has the scrubber, regenerative heat exchanger, air pump and control electronics all integrated into a single, compact unit.

The water boiler is intended to demonstrate how the larger power output of the VEM technique can be applied to a practical application. In this, the prototype simulates the concept of directly attaching the catalytic heating unit to a soldier-issued canteen.

Part of its purpose was to demonstrate that the integrated body of the catalytic heater can be detached from the water reservoir, thus allowing the unit to be used in providing heat power to other potential applications such as a hot plate, MRE heat-sheet, etc.

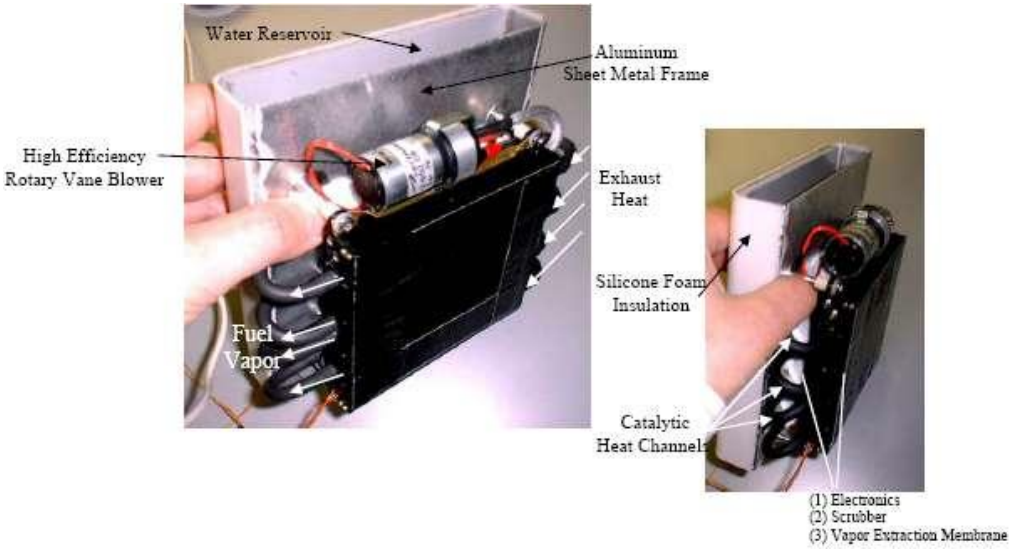

Figure 45. 300-Watt VEM Unit Demonstration

The unit shown utilizes porous membranes based on a long slender and hollow tube like geometry. This was illustrated in Figure 21 and Figure 28. The primary difference in this particular implementation, besides having all of the subsystems integrated into one single block, is the increase in the total surface area (i.e., number of tubes) of the tubular membrane. The unit worked well and provided over 300 watts of heat power to the water tank.

Because the VEM technique needs to have a continual source of auxiliary heat to drive the VEM membranes, the efficiency of the overall system is very dependent on keeping the unit compact so that the auxiliary heat goes into the vaporizer and is not lost incidentally to the rest of the system components or the environment in general. The theoretical minimum auxiliary power needed for methanol evaporation is about 5% of the chemical power in the vapor stream. Thus, a 100 watt VEM unit would need a theoretical minimum of 5 watts of heat power to drive the evaporation process. If no other losses are incurred, the system would, therefore, achieve a 95% efficiency. The 300-watt unit in Figure 45 achieved about 85% efficiency. That is, about 80% of the 300 watts of chemical potential power was delivered into the target (i.e., water in the tank). The efficiency of the phase-1 VEM units were even less efficient, but primarily because the coupling between the reactor elements and the hot plate was not ideal.

To increase efficiency and reduce system unit costs, a more compact version of the system shown Figure 45 was needed. Part of the higher than desired cost resulted from VEM membranes being made from e-PTFE, which is very costly. Another contributing factor was the assembly process being excessively complicated because the tube like structures were difficult to terminate in a hermetic manner.

Separate from cost factors, the use of tubular e-PTFE resulted in a larger than desired footprint, and a requirement that the methanol be diluted to a 90%-methanol/10%-water solution reduced the power density of the fuel. That is, the power per unit volume was less than might be obtained with other membrane geometries and membrane materials.

To remedy this, CDI performed a series of experiments to find a new material for the membranes. This resulted in a switch to a relatively inexpensive oleophobic planar membrane with a consequent redesign of the whole assembly to take advantage of its better properties.

The process began by testing the properties of the new planar membranes and building a test station to provide basic engineering information.

The membrane shown in **Figure 46** is a thin sheet of an oleophobic membrane selected for its density, porosity and thickness. It is less expensive to extrude sheet membranes compared to the tubular membranes used in the earlier VEM devices, and the oleophobic membranes were much more resistant to liquid-fuel penetration.

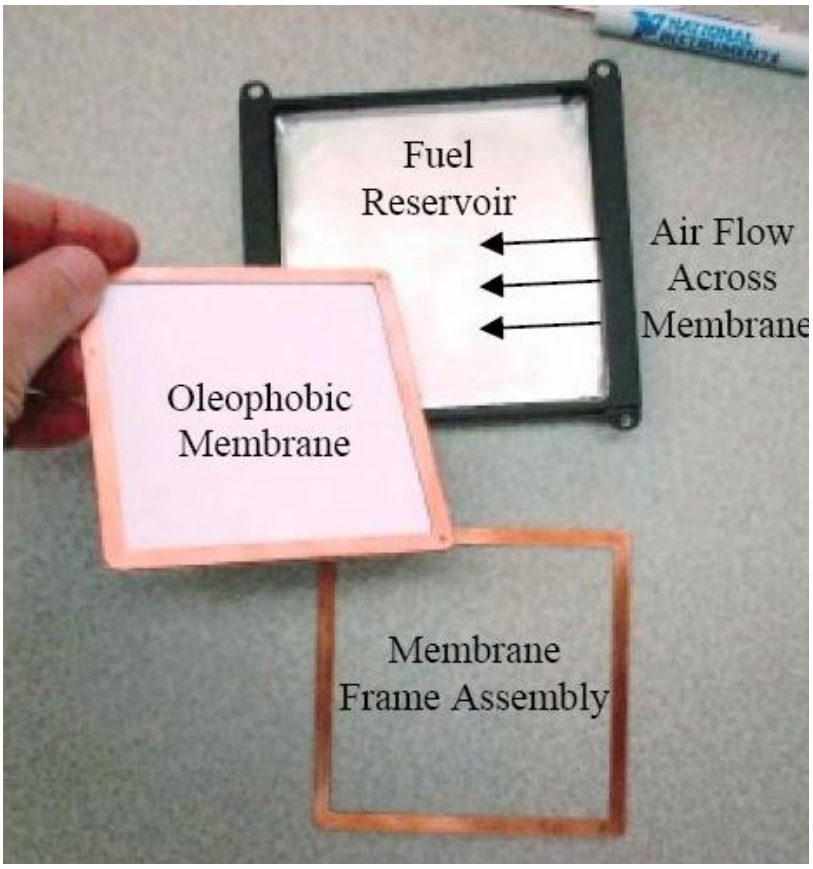

Figure 46. Test Cell for Planar Vapor-Exchange Membrane

The membrane is mounted in a frame that allows it to be held by the test cell where fuel and air are supplied as needed to test evaporation performance under different conditions. One of the factors that contributed to both the cost and degree of compactness the planar design can achieve is related to the rate of evaporation per unit area of membrane. This in turn is a function of both fundamental membrane properties and the air flow rate and fuel temperature.

Since evaporation occurs at the boundary layer of the membrane, boundary layer air flow conditions control the result in those cases that are not diffusion rate limited by the membrane itself.

To understand this and design the best VEM evaporator, a series of flow plates (**Figure 47**) were fabricated that alter the flow pattern in a known fashion. The figure shows two of the four different test cell lids that were designed and fabricated to fit on the test cell.

Each lid, when securely sealed to the air-flow-side of the test cell, will generate different airflow patterns near the boundary layer. These different flow patterns were then examined to see what there relationship is with vaporization rates and efficiencies.

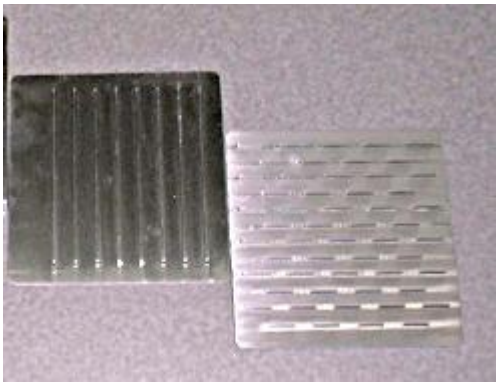

Figure 47. Planar Vapor-Exchange Membrane Flow Test Plates

Figure 48 compares the results of modifying the flow velocity over a fixed-area vapor extraction membrane. The top two curves are for comparison purposes; they represent data extracted from the earlier "tubular" membrane-type VEMs and help to interpret the results of the planar membrane performance. In principal, it should be possible to distinguish between the effects of surface area, flow velocity and turbulent mixing on the efficiency of vapor extraction across the membrane.

The bottom two curves, for instance, show how, while keeping the surface area constant, an increase in flow velocity increases the vapor extraction rate. An increase in the extraction rate is expected based merely on the fact that the boundary layer thickness is decreased. The degree to which this affects the extraction rate is seen by comparing the bottom curve with the curve just above it. About a 25% improvement in extraction rate occurs per unit area for the newer membrane.

From these experiments, it was possible to extract evaporation rate per unit area and flow-stream velocity dependence. This was then used to start the design for the next generation of VEM type technology where advantage is made of the natural stacking capability associated with planar type structure.

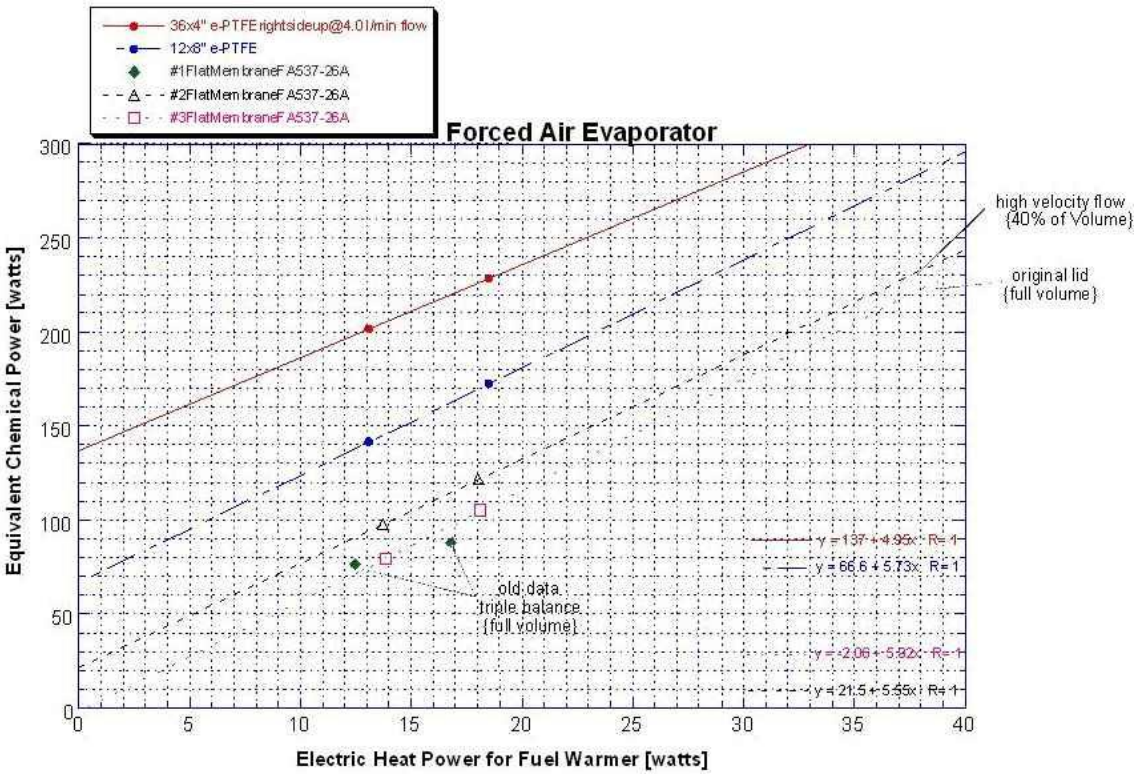

Figure 48. Results of Test Cell for Several Planar VEM Membranes

Figure 49 shows the exploded view of the new, stacked-membrane topology, VEM vaporizer. The stacked membrane unit consists of three stacked compartments forming a single module. Each compartment has two, 1 square-inch, vapor exchange membranes. This gives a total area of about 6 square inches -- even though the one-dimensional footprint is only 1 square-inch. A micro-fluidic fuel distributor plate feeds each of the three VEM compartments. Within each compartment is located a heat transfer plate that attaches to a micro-catalyst heater which is fed by diverting a small portion of the main fuel/air stream going to the heat sheets. This heat provides the heat-of-vaporization necessary to maintain the vaporization process.

The fuel is fed to the stacked membrane cells by a constant fluid-pressure mechanism within the fuel storage cartridge. **Figure 50** shows the results of early tests on the configuration shown in Figure 49. Data for two catalytic-housing setpoint temperatures is graphed. The rate at which fuel is vaporized is dependent on both the airflow rate and the temperature of the heat transfer plates which provide the energy required for continuous evaporation. The temperatures quoted in the graph are for the micro-catalyst heater housing temperature. A set of heat transfer plates,

attached from the micro-catalytic heater to the VEM stack, provide the thermal path for the heat energy. The temperature of the heat transfer plates is less than the micro-catalytic heater housing and is not uniform across the plate. The average temperature of the heat transfer plates is estimated to be at least 20 °F less than housing temperature.

The change in output power with operating temperature is related to the change in fuel saturation vapor pressure. The relationship, governed by the Clausius-Clapyron equation, is exponential with respect to temperature. A housing temperature of about 150 °F should give greater than 200 watts at the upper air flow rate (i.e., 2.5 liters/minutes).

This housing temperature should not be felt by the user since it is well within the handheld unit and the heat is constantly being carried away by the vaporized fuel, thus preventing the heat from flowing into the outer regions of the hand held unit. This is to be expected; for instance, the catalytically driven ceramic wick design demonstrated in December 2004 had an internal temperature of 250 °F and was not noticeable to the user.

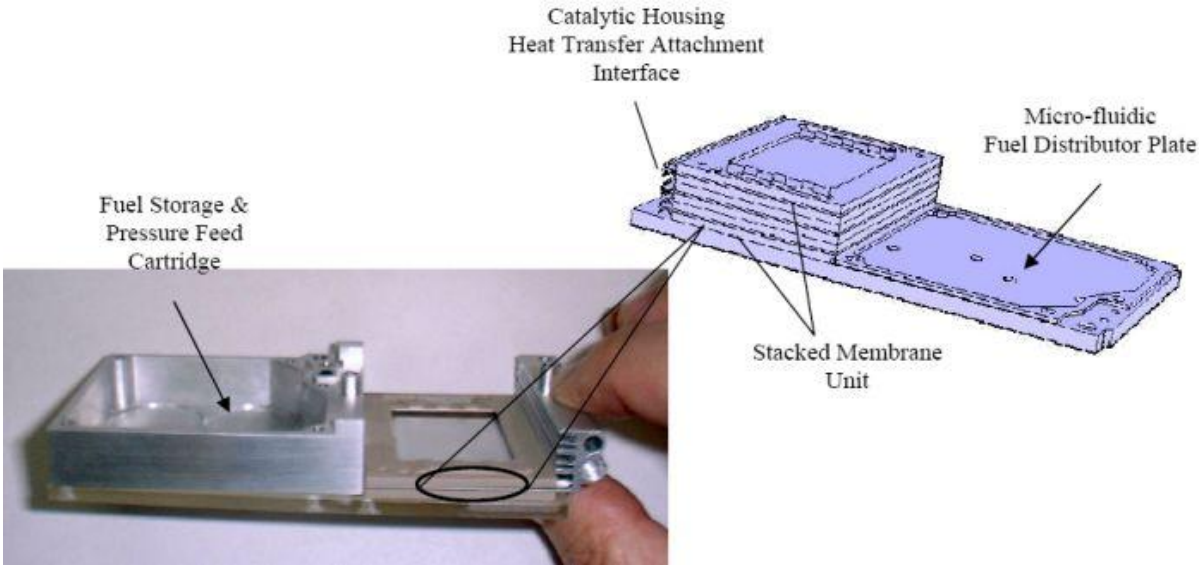

Figure 49. Stacked Membrane VEM Topology

It is worth noting that the total projected membrane area for this topology is about 3 square-inches and produces close to 200 watts at 2.5 l/min. Contrasting this with the early cooker that had 20 square-inches of membrane surface area for about the same power output, it is evident that significant progress in miniaturizing and lower costs has been obtained.

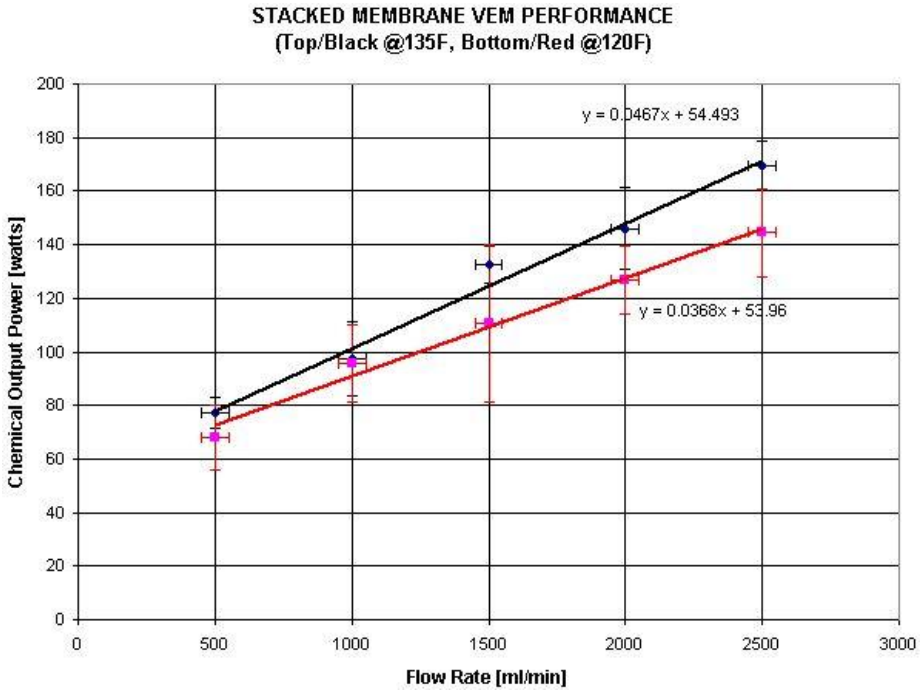

Figure 50. VEM Stack Performance with Oleophobic Membranes

The data show that at 2500 ml/minute total flowrate, the VEM stacked-cell unit contributes about 0.2 inches-H_2O of pressure drop. This is excellent performance and indicates that operating this VEM unit at much higher flowrates is feasible since it would place very little power demand on the air pump.

It also demonstrates that the majority of pressure drop comes from the fuel distributor plate. Besides delivering the liquid fuel to the VEM stacked cell unit, the fuel distributor plate is used to route an undiluted airflow stream from the air pump to the membranes, where fuel vapor extraction occurs.

To resolve this situation the cross-sectional area of the internal airflow channels within the plate was increased. This reduced the pressure drop to a value dependent solely on the VEM stack geometry, allowing the air pump power demand to be reduced substantially.

A third, more advance version of the VEM based vaporization approach was designed and constructed. It is far more compact and has all the subsystems fully integrated into a small by powerful package. This is shown **Figure 51** below.

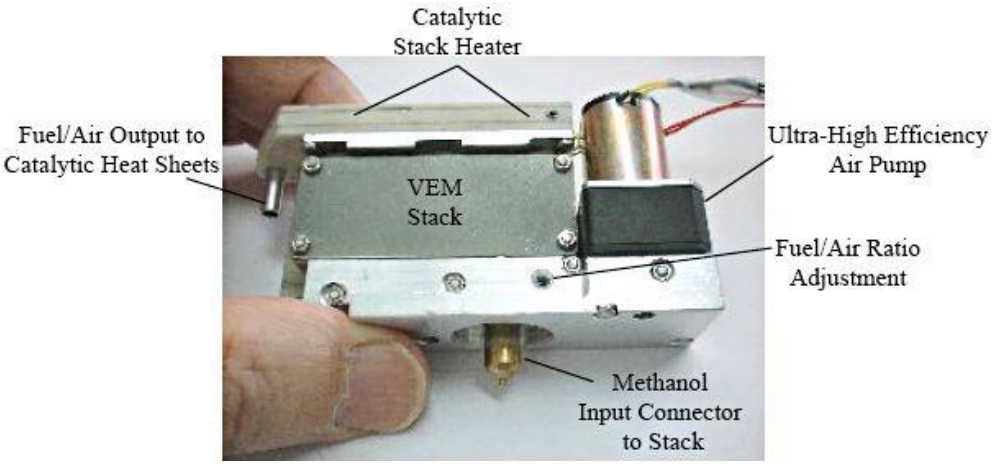

Figure 51. Fully Integrated & Miniaturized 75-Watt VEM System

This VEM unit has allows for manual adjustment of set-points for fuel/air ratio and operating temperature of the micro-catalytic stack heater. It also incorporates a high-efficiency air pump constructed from a graphite impregnated polymer to allow low friction without use of lubricants. This avoids any issues with lubricant migration into sensitive areas such as the micro-catalytic heater or the VEM stack.

3.1.2 Thermo-Capillary Evaporator

A new design concept for fuel vaporization and metering has been explored at CDI recently. The basic concept of using a "wick" as a fuel saturated surface and driving the fuel into the vapor state is not in itself new. In fact wicks as fuel vaporization schemes go back to antiquity (e.g., candles, torches, kerosene lamps, etc.).

However, in order to meet the operational requirements of the applications being pursued at CDI, a significant increase in the sophistication is required to employ the wick approach.

A simplified diagram of the concept is shown in **Figure 52**. This diagram shows a porous body (i.e., wick) that provides sufficient capillary action to overcome the expected hydraulic head (e.g., >4 inches-H_2O) needed to send fuel to the vapor generating surface. At the same time, the material must have sufficient permeability to allow sufficient fuel-delivery rate.

The top loop (from the exit end of the catalyst channel) was added to insure that minute changes in the back pressure of the MRE (i.e., the heat sheet) will not change the ratio of flows between the output to the reactor and the feedback flow to the micro-catalytic heater shown in the diagram. This is important for maintaining a proportional relationship between heat supplied for vaporization and the fuel demand by the MRE.

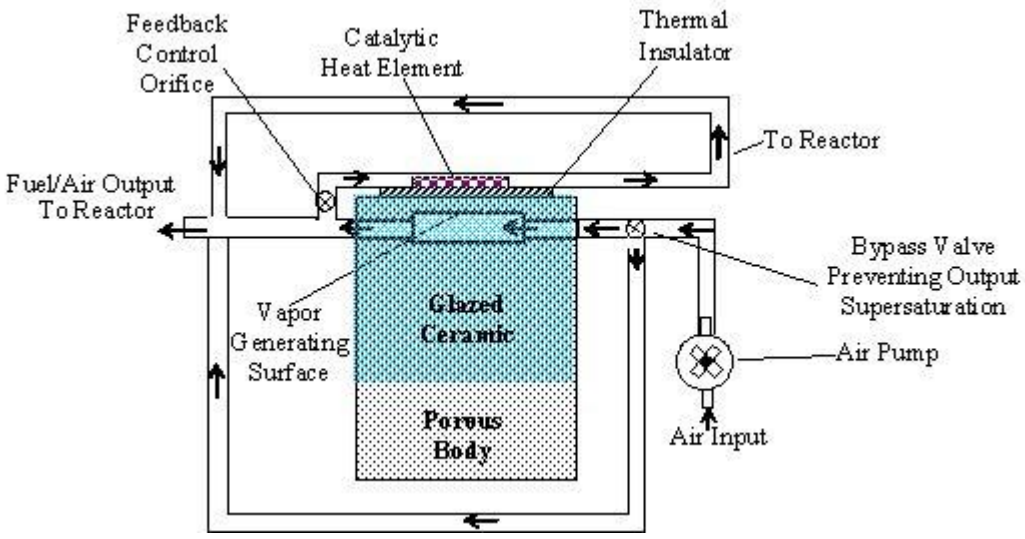

Figure 52. Catalytically-Driven Wick Evaporator

The thermal material properties and dimensions must be chosen to allow for correct heat transfer from the micro-catalytic heater to the vapor-generating surface and avoid nucleate boiling along the heat transfer path. At the same time, the heat output of the micro-catalytic heater must be kept within certain bounds at all times. In particular, when changing the equivalent chemical power output (i.e., fuel/air flow rate multiplied by heat of combustion per unit volume) of the device, the catalyst must not be over or under driven.

The bottom loop (from air input to output) provides air dilution of the main stream to insure the output is not supersaturated at any point in the operating range. This avoids fuel condensation in the miniature pneumatic feed lines going to the MRE. Overdriving the catalyst can cause the vapor-generating surface either to be "starved" of fuel (i.e., blocking capillary flow) or to produce supersaturated fuel/air mixtures with resultant condensation. To insure the device will be orientation independent, the vapor generating interior surface may be treated with a hydrophobic agent to render it liquid impenetrable.

Other ways discovered to avoid this problem include:

(a) filling the ceramic body with only enough fuel such that capillary back pressure prevents dripping when inverted, although this sacrifices fuel capacity (i.e. similar to the trade-off used in ink jet cartridges); and

(b) inserting a hydrophobic membrane into the vaporization cavity, held in position by the spring-like action of a rolled-up stainless mesh (or something similar). The ends are then sealed using epoxy.

These concepts were implemented in the proof-of-principle demonstrator shown in **Figure 53** and **Figure 54**. This unit was operated continuously for 4 hours at an output of 200-watts-equivalent chemical power without any problem in a very small lightweight package. More importantly, the energy output from the catalyst was linearly related to the MRE heat demand. This was critical to proper operation. It is anticipated that this unit, if used to drive the MRE heater, can bring the food up to temperature within five minutes or less. An additional motivation for pursuing this technical approach is rooted in the potential cost/performance gains that may be achieved.

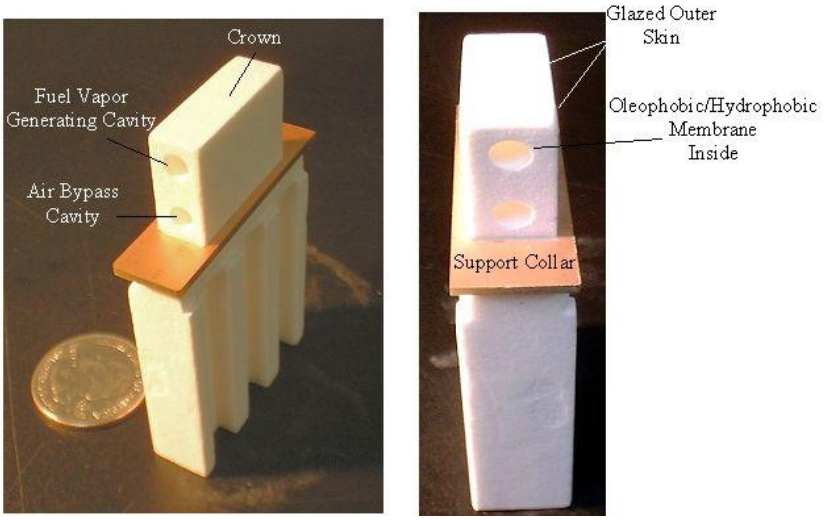

Figure 53. Thermo-Capillary Evaporator Assembly Details

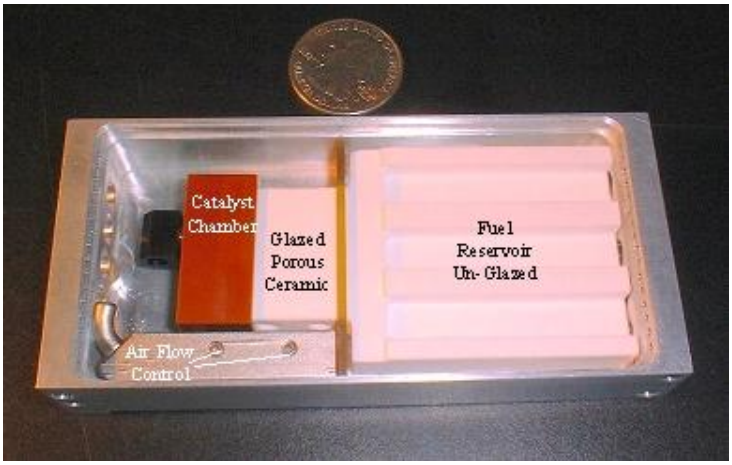

Figure 54. 3rd-Generation Wick Evaporator Prototype Packaged

The costs for this part of the system were expected to be much less than either the TIJ or vapor extraction membrane methods discussed in other parts of this report. This was based on both materials costs and fabrications costs estimates. However, toward the end of the project and after many variations on the theme, it was determined this was not true; the compact VEM approach turned out to be a lower cost and far more reliable approach. The reason for this has to do with certain complexities fabricating the thermo-capillary device and with some inherent functional sensitivities that would need to addressed to make it practical, for example:

(a) the seals around the ends of the hydrophobic barrier membrane were inherently week and prone to degradation;

(b) the fuel reservoir requires proper venting to allow equilibration of the pressure in the reservoir as the fuel leaves otherwise a vacuum forms which inhibits fuel flow. This vent needs to be open only when the device is active and closed when it is off to prevent a slow loss of fuel over time;

(c) the crown portion of the ceramic need to have a thin glaze over the outside surfaces only, and the glaze must perfect without pin holes;

(d) the seal between support collar, the crown and the fuel reservoir must be perfect but tends to be week and degrade over time; and

(e) the whole assembly requires shock proofing to avoid inducing micro-stress cracks over time.

These and many other similar small issues requires relatively costly engineering work-arounds which increase assembly cost greatly.

3.2 Catalytic Heat Sheet Designs

3.2.1 Embedded Autonomous Flex Channels

Figure 55 below shows the general morphology of a special type of the catalytic heat-channel. They are flexible and autonomous structures that can be molded into a base layer matrix. Depending on the application, the matrix material may consist of a polymer/multi-layer composite or some other material compatible with the service temperature of the channel materials. Alternatively, the channels could also be used as is, without imbedding into a support structure, because they are self-supporting and very rugged. They are relatively easy to manufacture and their mechanical compliance (i.e., flexibility) allows them to fit into complex geometries if needed.

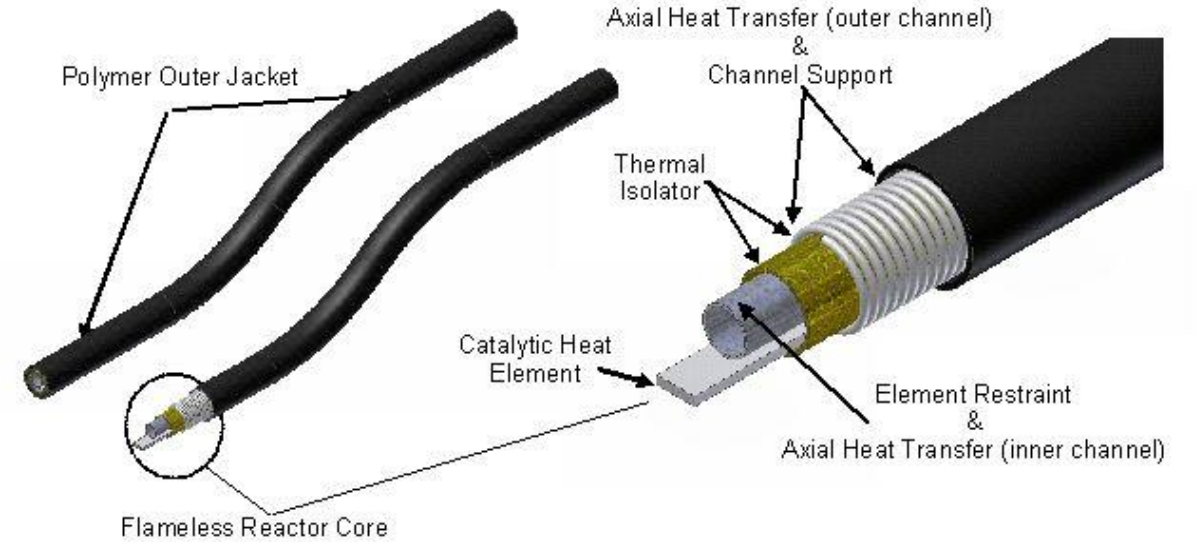

Figure 55. Autonomous Flexible Heat Channel Design Structure

The left side of Figure 55 shows the outer jacket material, which consists of a high temperature flexible polymer. The catalytic reaction takes place within the jacket at the reactor core. The right side of the figure shows a more detailed cut-away view of the core structure. The channel support, just below the outer jacket, performs an important heat transfer function.

In general, the channel support consists of a relatively high thermal conductivity material -- such as steel, aluminum, or copper -- that can provide suitable strength at the elevated operating temperatures. The pitch of the channel support (i.e., the number of coils per unit length) can be varied as needed for a particular application. In some configurations it may be advantageous to change the pitch along the axis of the channel to enhance uniformity of the axial temperature profile.

Below the channel support is an optional thermal isolator that performs the function of further "tuning" the heat transfer process along the length of the channel. An expanded foil insert is added within the thermal isolator to provide a restraint for the catalytic heat element and also performs as an "inner channel" axial heat-transfer enhancement device.

The left side of **Figure 56** illustrates the placement of the autonomous heat channels embedded in a flexible polymer matrix. A heat diffusing woven copper sheet is co-molded with the heat channels. The woven metal enhances lateral heat diffusion across the surface of the sheet to improve uniformity of the temperature profile without interfering with the flexibility of the sheet.

The right side of Figure 56 is a photo of a working prototype incorporating autonomous heat elements. In this case, the matrix chosen is an unfilled, platinum cured, silicone rubber compound. The woven copper heat diffuser is co-molded during the silicone matrix formation. In this prototype, the heat sheet contains two active heat-generating channels.

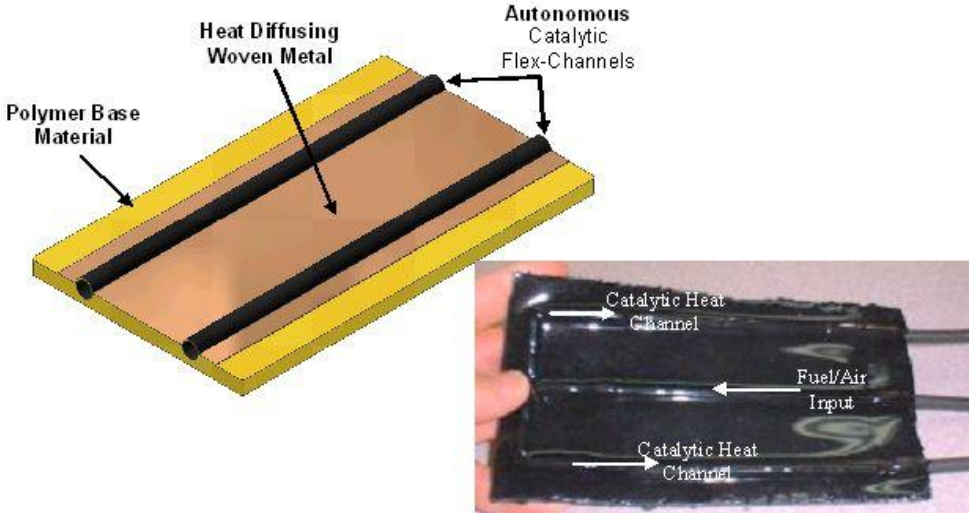

Figure 56. Autonomous Catalytic Heat Channels Embedded

Figure 57 shows a time-lapsed series of thermal images of the heat sheet on the right side of Figure 56. An infrared thermal imaging camera from Irisys (model IRI-1001) was utilized to capture the temperature profile across the sheet.

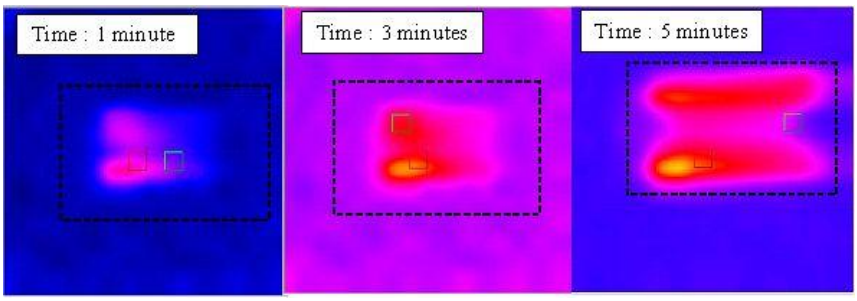

Figure 57. Time-Lapsed Infra-Red Temperature Profiles

The time sequence of images demonstrates that the bottom heat channel starts first and shows it beginning to extend its temperature profile along its whole length. At the 3-minute mark, the image shows a hot-spot starting to form at the entrance to the bottom heat channel. The five-minute mark thermal image presents a temperature profile across the sheet that is not completely uniform. The hot-spot is still visible in the bottom channel.

The temperature of the heat sheet further away from the channels differs from the average heat channel temperature by about 30 °C. This is attributed to insufficient coupling of the heat channels to the woven copper heat diffuser. Later versions improved this value to about 10 °C. Additionally, the channel profiles were changed to rectangular so as to better accommodate the thin sheet format desired in this application.

3.2.2 Semi-Ridged Segmented Channels

Figure 58 illustrates an alternative design for the autonomous flex channel concept. It incorporates several modifications of the concept shown above.

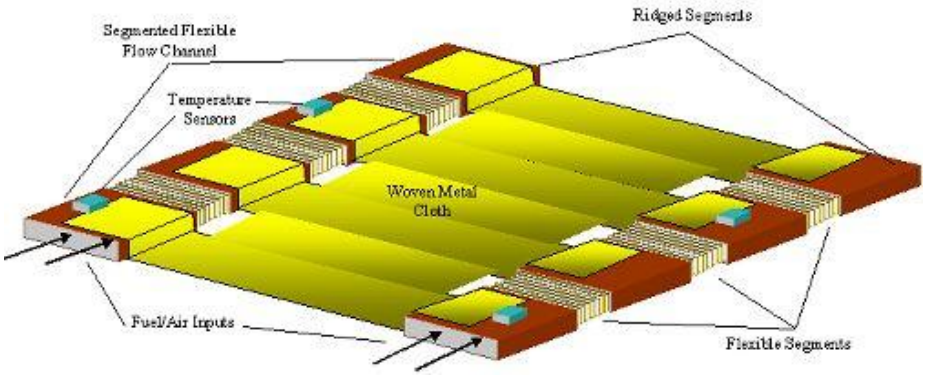

Figure 58. Alternative Heat Sheet Design Concept

The changes include:

(a) thin profile channels (i.e., rectangular),
(b) combined ridged and flexible segments to produce an overall flexible channel with good heat transfer from the ridged segments, and
(c) reduced number of sensors.

The flexible segments are made from rectangular springs coated with a polymer jacket. The whole assembly is then coated in a thin polymer layer to provide physical integrity and allow the silicone gel layer to have a suitable attachment surface.

The thin profile inherent in this design not only allows the lower overall weight, but also helps to enhance mechanical flexibility and lateral heat transfer across the sheet. The lateral heat-transfer is improved substantially because the solid segments allow better coupling of the heat energy to the woven metal layer. While this design had some excellent performance properties, it was determined to be too labor intensive and prone to a variety of fabrication issues. This resulted in a low yield and high cost.

A third variation was attempted that ultimately was shown to have the right combination of properties to allow for a reliable, cost effective and readily manufacturable heat sheet while maintaining all of the best functionality. This is discussed in the next section.

3.2.3 Integrated Iso-Planar Flex Channels

The fabrication and economic benefits derived from the concept of iso-planar construction has its origins in the early days of the semi-conductor industry. Although the original rational was directed toward solving certain electrical reliability problems, the resulting monolithic structures became the basis for a new economic model in fabrication efficiencies within that industry.

Borrowing this concept and applying it to heat sheet construction will also result in some economic and reliability improvements. In the case of catalytic heat sheets, the idea is to place as much as practical of the component functionality into a single layer.

The approach that turned out to be most successful is shown **Figure 59**. This construction consists of two substructures. The first is the active layer; it consists of a nearly iso-planar layering of a (a) sensor array and flex circuit, (b) isolation layer, (c) heat diffusion layer, and (d) bottom isolation layer. Total thickness of the layer is about one half millimeter.

The second layer is the bottom passive layer containing all the flow channel structures for directing the fuel/air mixture to appropriate areas within. It's made from a thin sheet of flexible elastomeric material about three or four millimeters thick. The catalytic heat elements are not part of these structures but rather inserted in a separate operation after both top and bottom layers are attached to each other.

All materials are chosen so that the heat sheet is capable of operating up to a temperature of 350 °F (150 °C). For purposes of cooking, this more than ample. For many applications, the heat sheet temperature would operate well below this value.

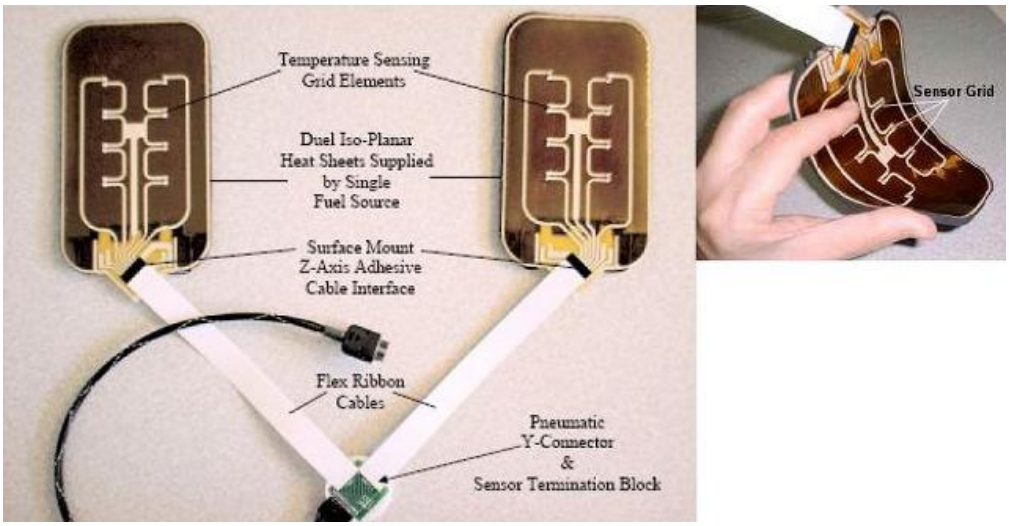

Figure 59. Duel Catalytic Heat Sheet Design

3.2.4 MRE Form and Function

The MRE form and function is partly determined by choice of subsystems. The subsystems evolved substantially during the project. During phase 2 their development reached a point where each subsystem achieved a high level performance, coming close to best form, fit and function.

Viewed in this way, the natural choices for the MRE prototype subsystems are: (a) VEM planar stack evaporation system, (b) iso-planar heat sheet construction, and (c) MCU based electronics control.

Figure 60 shows an early prototype for an MRE food packet heat generating envelope. The envelope consists of an outer layer of polyimide film upon which is attached a light weight silicone foam base. The base has recessed contours so that it will hold the heat generating elements. The recess containing the heat elements is back-filled with a silicone gel material.

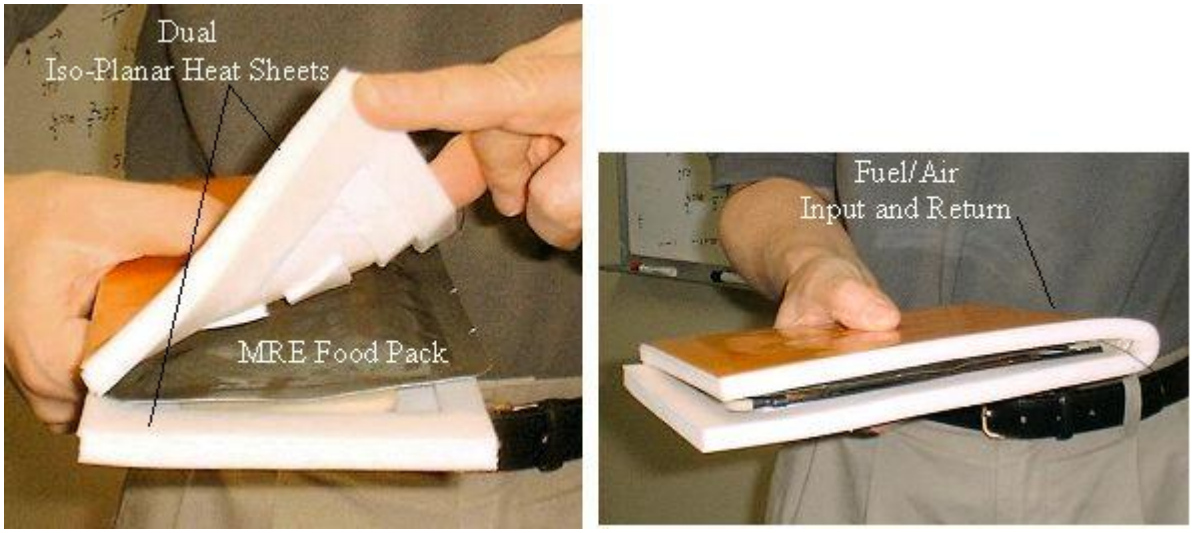

Figure 60. 3rd-Generation Wick Evaporator Prototype Packaged

The purpose of the gel is to adhere to the surface of the food pack during heating so air gaps are not formed. It has been calculated a net increase of the heat transfer will occur if the air gaps are substantially limited. This happens because the thermal conductivity of the gel is far more than the thermal conductivity of air.

Unfortunately, the silicone-gel curing cycle is sensitive to a wide number of common environmental constituents such as paper and wood products, latex gloves, some epoxies, etc. This resulted in portions of the gel being too sticky or containing pockets of subsurface uncured gel. In addition, over time, the gel attracts minute fragments of dirt and debris reducing its effectiveness. This first prototype allowed useful engineering data to be generated but lacked some of the additional features required to make it practical.

Because of these difficulties, the decision was made to redesign the MRE heater without the gap-filling gel component. This is shown in **Figure 61**. The MRE heater design has a thick insulating outer shell that can be closed using a zipper attachment. The heat-sheets slip into pockets that are formed in the shell and held in place with elastic bands. On the opposite side of the shell (not shown in the figure) is another smaller zippered pocket that contains the generator unit. The generator unit contains the vaporizer and control electronics and is connected to the heat sheets using flat flex-cable and a special hinged pneumatic connector.

To successfully complete the MRE, it was necessary to come up with some way to direct the fuel/air stream into both the top and bottom heat sheets while allowing the soft shell to open and close easily. This function required the development of a special hinged pneumatic connector that allows the fuel/air mixture to be directed into both the upper and lower heat sheets.

Figure 62 shows a close-up view of the hinged pneumatic connector arrived at after several attempts. It has one input and output located at the top where the generator output and return lines connect. Each hinged half has a central output surrounded by two return paths from the heat sheet. This arrangement is determined solely by internal channel design of the heat sheets and could be changed if other internal channel designs are used in the future.

Figure 61. Re-Usable MRE Heater

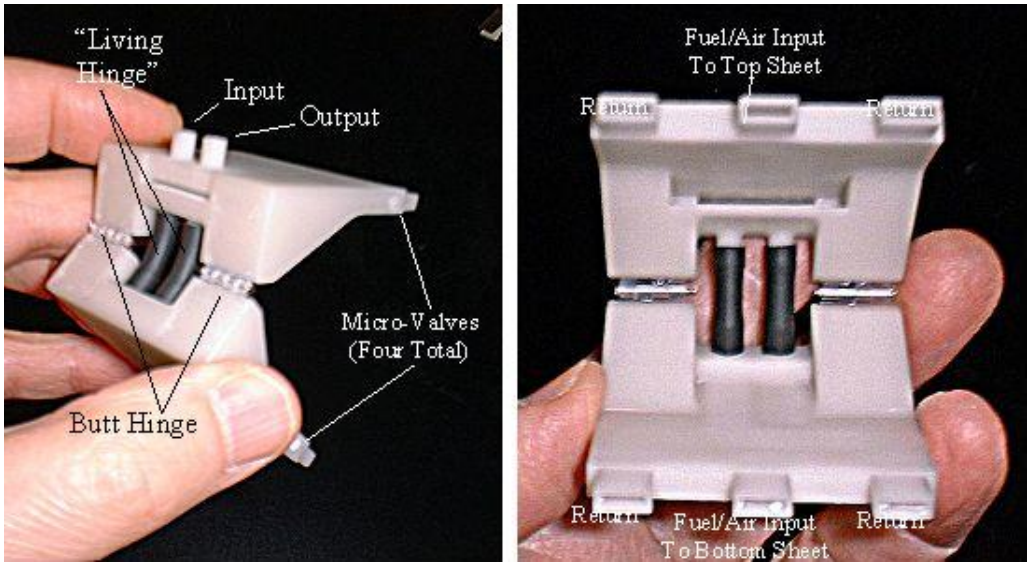

Figure 62. Hinged Pneumatic Connector

Figure 63 shows the data collected for measuring the rate of temperature rise at the center of a typical eight-ounce entrée in an MRE. The top curve differed from the bottom curve only in that the heat sheets and food pack were inside of the thick insulated envelop shown in Figure 61.

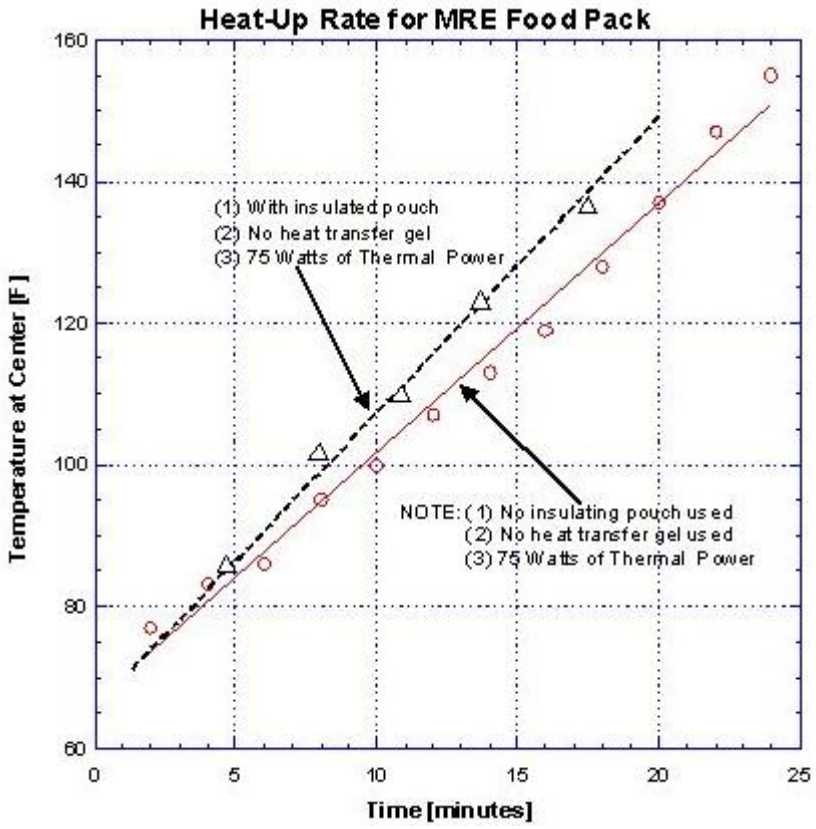

Figure 63. Heat-Up Rate for MRE Heater

The benefits of the insulation are clearly shown in terms of the increase slope of the curve. The heat power was set at 75 watts, resulting in a ready-to-eat temperature in about 12 minutes. Faster heat-up rates are easily obtained by increasing the heat power output of the VEM vaporization unit.

However, one constraint not obvious from the temperature curves is that the food packs are wrapped in a layer of thermal plastic. A thermal gradient must be established to drive heat energy toward a temperature sink. If an increase in the heating rate is achieved by arbitrarily raising the input heat power, the thermal gradient will increase to accommodate the input power increase. At some point, the MRE entrée surface temperature will increase to a value which might melt the wrapping spoiling or deteriorating the food. The thermal plastic surface temperature must not exceed 160 °F.

Some measures that can be employed to increase the heat-up rate and avoid high surface temperatures, include insuring good thermal contact with the packet and maximizing the surface area over which the heat energy is delivered to the packet. Of course, supplying heat in the center of the food packet would give the greatest advantage since the thermal gradient would be

inverted and the packet surface temperature would be lower than the central temperature. Although this can be done with microwave heating and specialized electrical heating (e.g., an inert resistance-foil packaged with the food), in general it is not feasible with most heat sources designed for external heat energy delivery.

3.3 Electronics Development

The electrical controls evolved throughout the project. **Figure 64** illustrates the apparent size changes that occurred. This was driven not only by the need to continue to shrink the system, but also the desire to minimize cost and complexity.

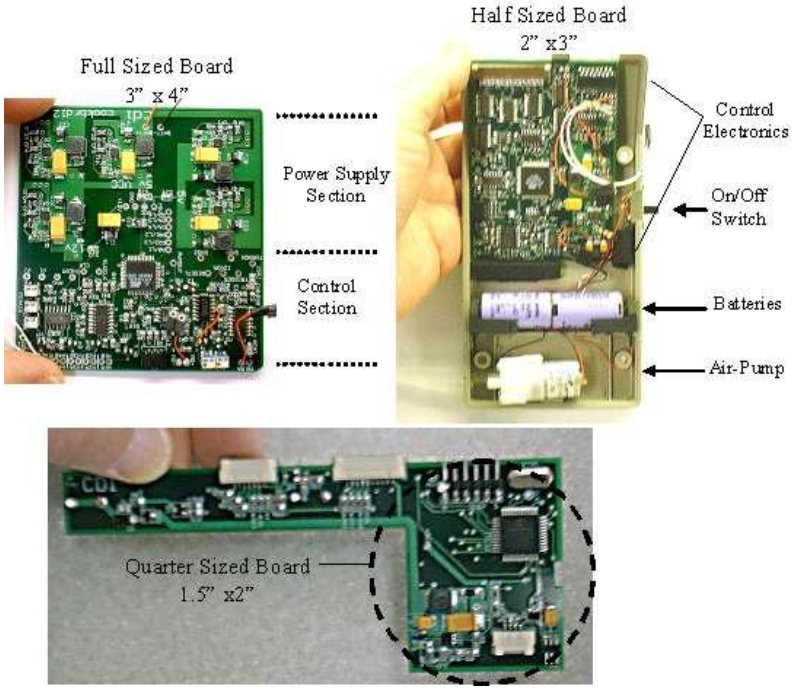

Figure 64. Evolution of Electronics Control Subsystem

The early stages of the project were centered around using a CPLD chip as the primary logic controller—chosen to comply with the need for a real-time control of the TIJ firing sequence. This is shown in the upper left photo of Figure 64. Eventually, because of the need for higher density in the logic, the core chip was changed to an FPGA. This provided not only the miniaturization, but also a reduced programming complexity. This is shown in the upper right photo.

In the natural course of development, it was determined that the TIJ approach should be replaced by the VEM system of vaporization. The VEM approach does not require a real-time operating system; therefore, it was determined that the needs of the system electronics were better served by moving to an MCU device. The MCU provided an even higher level of integration, better software development environment and an improved user interface for the software designer.

An example of board space reduction using an MCU strategy is shown in the lower photo of Figure 64. By moving to the MCU, many of the peripheral chips were eliminated because the MCU contains on board analog-to-digital converters, pulse-width-modulation outputs, and a variety of built-in serial communication capability.

When a real-time operating response is desirable, the MCU-based logic can be brought by varying degrees to this level of performance by using a variety of methods ranging from simple interrupt-driven state-machine software at the low end of complexity, to incorporating a full real-time operating system kernel in the software environment at the high end. The choice would depend on how strict the definition of real-time needs to be. Thus, the MCU provides the flexibility to grow with the system design without significant changes in the platform or development tools.

The modern MCU also has a variety of methods to reduce on-board power consumption by including "sleep mode" and/or simply operating at very low clock speeds. The latest MCUs can achieve nanowatt-type power consumption during the sleep cycle. These capabilities are advantageous for promoting very long battery life.

3.4 Supporting Technical Efforts

In any long-term project, a number of technical efforts may need to be undertaken that were not originally planned. This results from the fact it is not possible to entirely predict direction of a new technical development, which by its very nature will reveal previously unknown facts about the nature of the underlying phenomenon. These supporting tasks are discussed in this section.

It was determined earlier in the project that although the catalytic micro-plate heater used in the TIJ approach to fuel vaporization and metering was successful, its efficiency was far less than anticipated. An effort was undertaken to dramatically improve the efficiency.

Figure 65 illustrates the overall result of improving the efficiency of the catalytic micro-plate heater. In this case the efficiency improvement results from both increasing overall transfer of heat from the micro-plate to the fuel droplets and reducing electrical power required to start the vaporization process. In operation, once the catalytic portion of the micro-plate heater starts contributing sufficient heat, the electrically driven portion is powered back or completely turned off to conserve battery life.

The wide operating domain for the new micro-plate heater (as shown in **Figure 66** illustrating the key physical principles behind the efficiency increase), is due to the non-periodic nature of the starting vaporization supply current. The non-periodic nature derives from the fact that electric power is supplied to the heater only when the catalytic self heating is not providing sufficient energy. This scheme is done to avoid having the catalytic self heat contribution overdrive the micro-plate, causing large temperature excursions.

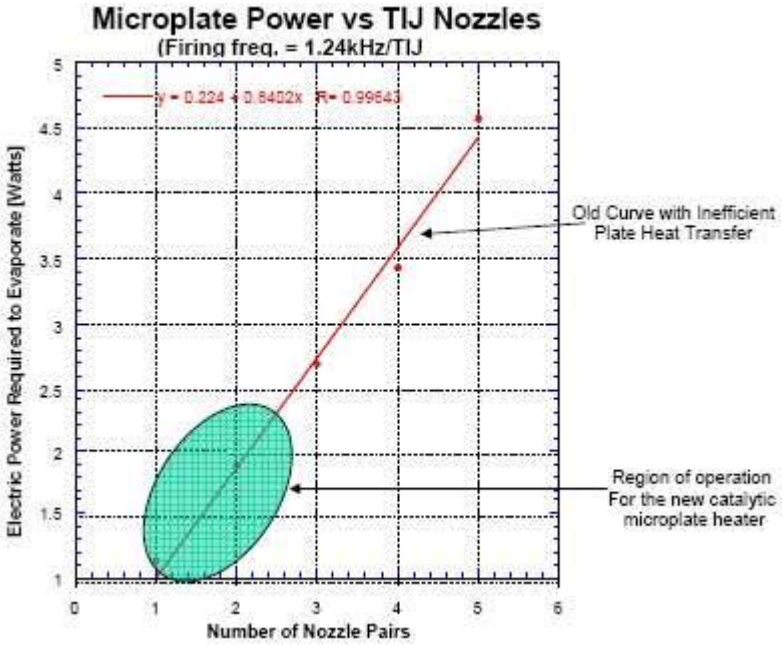

Figure 65. Power Curve Comparison of Improved Micro-Plate

In the old method, each fuel droplet would "float" on a gas film that is generated at the moment of contact with the hot micro-plate surface. The gas film, which consists largely of vaporized fuel, impeded the transfer of heat from the micro-plate to the fuel droplet. This results in the need for much higher micro-plate power levels to vaporize a given quantity of fuel per unit time

To eliminate the insulating gas barrier, a new method was established where the droplet is immediately made to spread out and become trapped in small pockets which are filled through capillary action. The pockets force the droplets to increase the contact area with the micro-plate heater. The result is a highly improved transfer efficiency of heat to the droplet allowing much lower micro-plate surface temperatures for a given fuel evaporation rate.

A portion of the vaporized fuel/air stream is routed away from the targeted heat sheet and sent underneath the micro-plate where a strip of catalyst reacts fuel/air vapor to provide additional heat to the micro-plate. This allows electrical power to be turned off entirely, essential after a short start-up sequence.

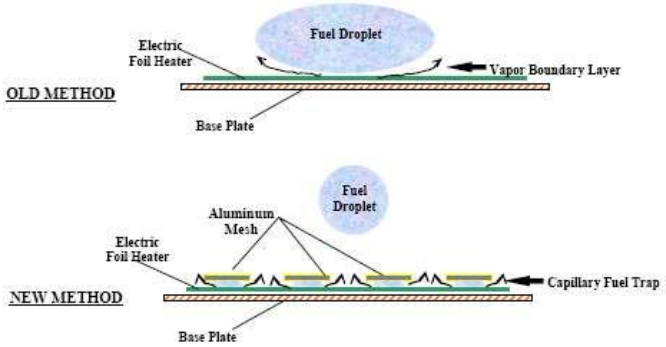

Figure 66. Improved Heat Transfer Micro-Plate Design

Because the micro-plate base is much thinner (~20 mils) than it is wide, the heat transfer from the back-side to the front-side has a low thermal resistance compared to the thermal resistance between the connecting base plate and the outside environment. This ensures the heat generated by the micro-plate is used almost entirely for vaporization and not heating up other system components.

The TIJ performance characteristics needed to be optimized for this application. This was done by experimenting with alterations of some of its components. For instance, **Figure 67** illustrates how physical modification to the fuel reservoir sponge properties can enhance TIJ performance. The principal purpose of the sponge material is to provide a negative capillary pressure (suction) to the fuel, compensating for the fuel hydraulic pressure head. Excessive gravity pressure head tends to ooze droplets from the TIJ nozzles.

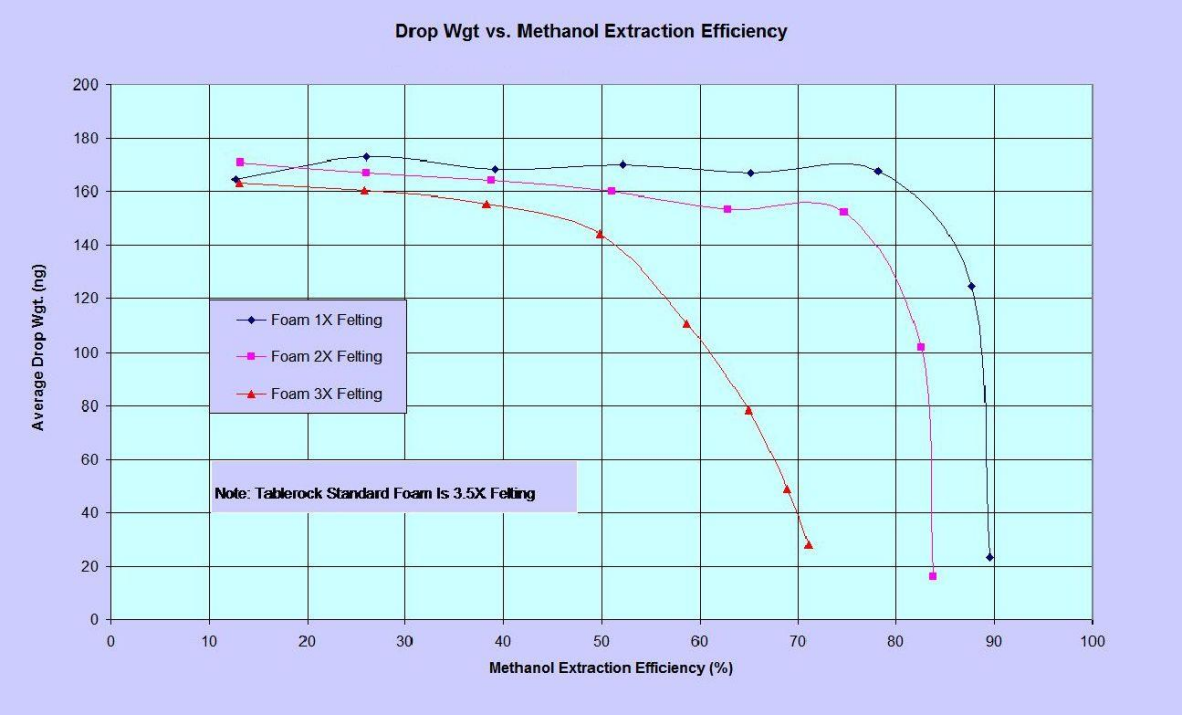

Figure 67. Felting Effect on Thermal Ink-Jet Properties

This is accomplished by varying the pore size within the sponge material in special ways. In particular, the sponge properties known as "reticulation" and "felting" are adjusted. Reticulation refers to the process whereby the pore walls are partially removed so fuel can move between and through adjacent pores.

Felting refers to the process of permanently compressing the sponge volume from its initial size to increase the number of pores per unit volume. The smaller pore size produces a larger backpressure. Proper adjustment of the pore size is determined by examining the trade-off between backpressure and percent of fuel that remains within the sponge at end of use. Figure 67 categorizes this effect under the heading “Methanol Extraction Efficiency” as shown along the abscissa.

The result is that if the backpressure chosen is too low, the TIJ nozzles will leak (dribble) fuel unless the hydraulic head is very small (i.e., small fuel reservoir). However, a low backpressure has the benefit that most of the fuel in the reservoir is available to be used (i.e., less residual fuel).

If, on the other hand, the backpressure is too high, the TIJ will not leak but might de-prime as the fuel volume decreases (i.e. less hydraulic head). A higher backpressure has the benefit that the fuel reservoir can be made larger without worrying about fuel dribble.

In general the correct choice of felting number for the particular application is dependent upon a number of trade-offs that will affect many important operational parameters. The optimum choice for CDI's application can now be determined using the chart in Figure 65.

Toward the end of the project it was determined that manufacturing of the catalytic heat elements resulted in certain characteristics having poor repeatability. A project was started to remedy this issue. In particular, it was known from first principles that catalyst concentration profiles along the heat elements will affect temperature profiles observed in the operational heat sheets.

Figure 68 shows spatial temperature profiles taken across two different heat elements with each element having a different axial concentration gradient of the Platinum catalyst. Previous to this, the catalyst was deposited uniformly and a spatial concentration gradient was obtained by applying an inhibitor using a manual application. The dose of the inhibitor at each position along the element was adjusted by hand. This was tedious and prone to inaccuracies.

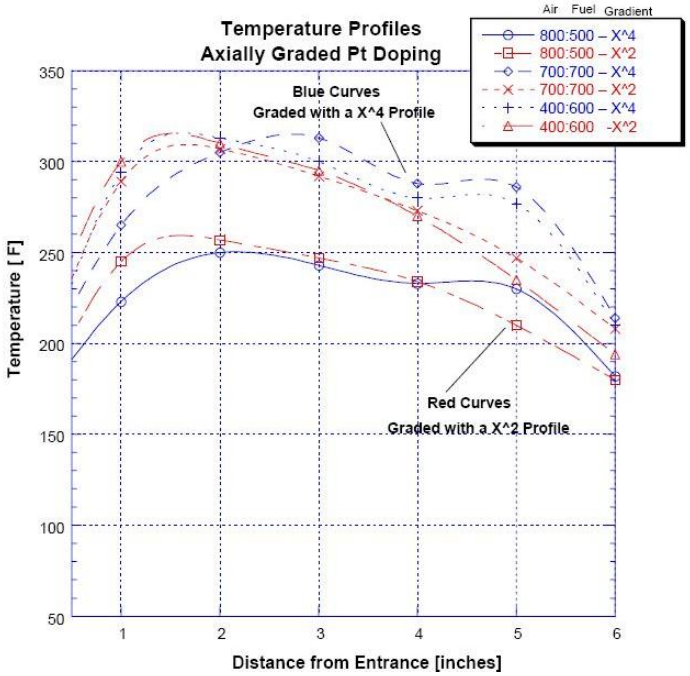

Figure 68. Pt Gradient Effect on Thermal Profiles

A newer, more precise and repeatable approach was needed. This was obtained by employing an X-Y plotter and inkjet cartridge filled with a platinum (Pt) solution. The solution was ejected from the TIJ micro-nozzles under computer control. Using a pre-determined pattern, microscopic droplets of the Pt solution are deposited on the heat element substrate and allowed to dry. They are then annealed in a hydrogen reducing furnace to activate the Pt solution.

The concentration was engineered so that one element had a 2^{nd} power dependence and the other had a 4^{th} power dependence. That is, starting at one end of the heat element, the concentration of Pt per unit area increases at a rate that depends on the axial distance along the element, resulting in a concentration gradient dependent on either the 2^{nd} power or 4^{th} power of axial position. The purpose of this is to spatially modulate the catalytic activity in such a manner as to counteract the natural tendency of the combustion process (i.e., flameless combustion) to collapse toward the fuel/air entrance.

Temperature was measured along the axis of the heat elements as a function of both time and fuel/air ratio. The time is relevant because it takes a while for the combustion process to reach equilibrium. Increasing fuel/air ratio shows an increase in the tendency of the collapse mechanism, and is thus a good indicator of how well the spatially modulated activity profile counteracts the collapse.

It is clear from Figure 68 that the 4^{th}-power curve reaches a stable condition that is spatially more uniform in temperature profile than the 2^{nd}-power curve, all though neither is entirely perfect. When the same elements are compared at either high fuel/air ratios and/or increased total-flow rates, the 4^{th}-power curve shows a substantially improved temperature profile.

The meaning of the air and fuel columns in the legend is as follows. "Air" refers to the flow rate of a pure air stream (i.e., no fuel vapor) used to dilute a separate flow stream. The separate flow stream is labeled "fuel". In practice, the fuel flow stream is generated by passing an air stream over a bath of methanol that is temperature stabilized at 26°C. This causes the air to become saturated with methanol; thus, 500:500 means 500 ml/minute pure air and 500 ml/minute saturated fuel/air. This allows the control fuel/air ratios to be precisely controlled.

The fuel/air entrance is labeled 0 inches. This is where the catalytic combustion collapse will naturally want to occur. The phenomenon of collapse, while well known to those who practice catalytic combustion in heterogeneous reactor configurations, has a fairly complex mechanism and has never been fully modeled in the literature.

Heuristically, it is useful to think of it as consisting of several interacting phenomenon, specifically:

> (a) a catalytic activity that is exponentially dependent on temperature in the low temperature regime (e.g. 100°C to ≈ 800°C);
> (b) a control volume (choose any small size) of fuel/air vapor moving in the stream that becomes more lean as it moves through the channel; and

(c) a hot combustion products that are acting to increase back pressure and pre-heat the nascent fuel vapor stream.

All these effects promote a movement of the reaction zone toward the entrance.

This deposition method for the heat elements used in Figure 68, shows promise to eliminate the need for an inhibitor and to allow for an automated, production worthy method of heat element fabrication that reduces the total amount of Pt required per heat element while increasing repeatability.

3.5 Safety/Hazards Review

Figure 69 through **Figure 71** presents the flame propagation velocity for particular combustible species as a function of volume percent mixture with air.

A general approach to safety analysis starts by contemplating potential hazard scenarios and assessing their potential for causing harm to human beings. Specifically, the procedure that CDI has implemented for safety evaluation are outlined as follows:

1. Identification of potential hazards.
2. Identification of possible mishaps that might couple with the potential hazards.
3. Elimination of as many hazards as possible.
4. Mitigation of identified potential mishaps

For the purposes of this project, the distinction between hazard and mishap is one of hierarchy. A hazard identifies a general category of potential danger, such as flammability. A mishap addresses the various possible groupings of event-sequences where ignition of the fuel/air mixture might exhibit itself. Generally, mishaps are organized in the order of high probability to low probability.

HAZARD #1: Flammability

One of the safety issues for any flameless combustion process is what happens if by some means, as yet unknown, the fuel air mixture is ignited. To produce a flame it is necessary to have a (a) flammable mixture, (b) source of ignition, and (c) conditions for a stable flame.

Item (a) is determined by the chemical species used for the fuel. For the case of methanol, the fuel air mixture must be above 6% by volume to achieve a flame -- assuming an ignition source is available. If the system were designed to run at 6% or below, no flame could ever be established. For purposes of system efficiency, it may desirable to run the system at a 13% (i.e., stoichiometric value) fuel/air mixture or by some mishap, the fuel/air mixture accidentally becomes more rich than the 6% lower flammability limit. In either case it becomes important as to how a flame front would behave if it were somehow established within the system.

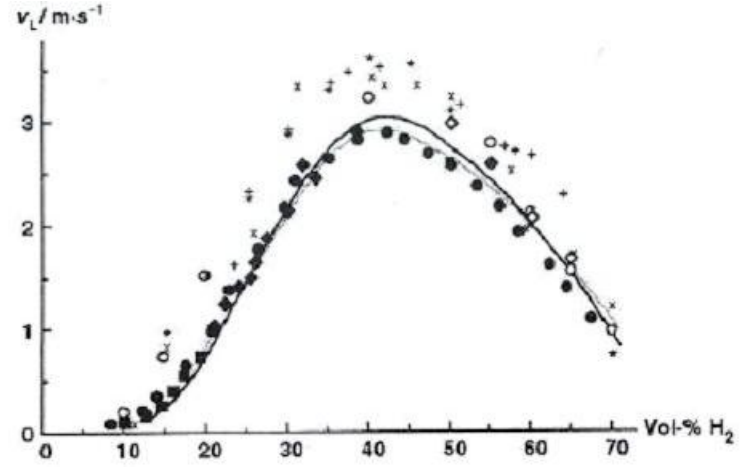

Figure 69. Flame Front Propagation Velocity for Hydrogen

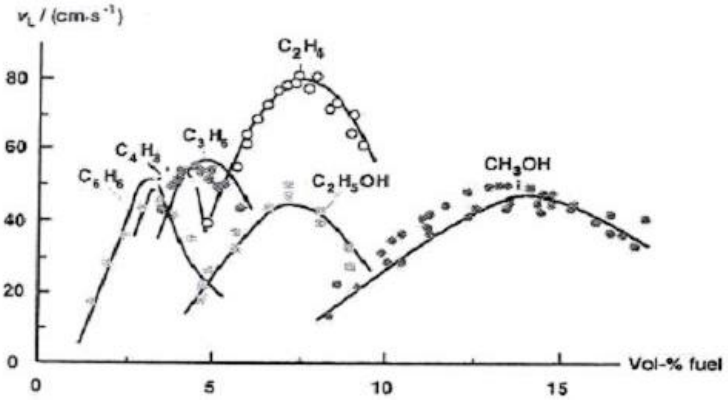

Figure 70. Flame Front Propagation Velocity of VOC's

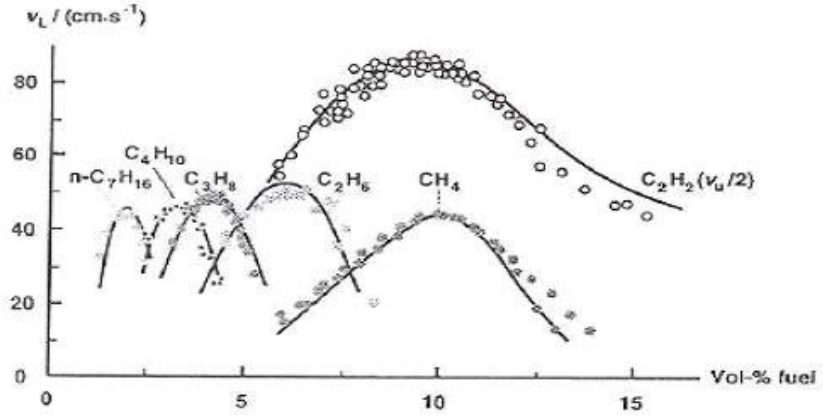

Figure 71. Flame Front Propagation Velocity of VOC's (continued)

Once a flame is started, it tends to propagate toward the fuel source. However, if the natural flame propagation velocity (different for each fuel) is less than the fuel/air stream velocity, then the flame is inhibited from moving toward the fuel source.

Figure 69 though Figure 71 may be used as examples of the wide variance in flame front propagation velocity that may be encountered depending on the fuel source and the fuel/air ratio. In particular, it should be noted that a methanol fuel/air mixture (i.e., CH_3OH) has a flame speed always less than 50 cm/sec. This value can then be compared to feed stream speeds found in AFCT technology. For the AFCT system, the lowest feed stream speed of fuel/air that is directed toward and through the channels containing catalyst, is generally above this value at all times during normal operation.

The next question to be answered concerns what will happen if the feed stream was accidentally interrupted (e.g., becomes static) causing a lowering of the stream speed to a value below the flame propagation speed. If this happens and a flame is somehow initiated by some unknown source, then the flame will propagate toward the fuel source.

Abnormal and unusual conditions like this can be remedied by examining in more detail the requirements for a stable flame. There are two fundamental conditions for a stable flame. They are that the (a) flame speed equals the fuel stream speed, and (b) channel size is greater than a critical number known as the quenching diameter.

Item (b), the quenching diameter, is shown in **Figure 72** for several different common combustible gases. It is noted that in general, the trend is that high flame propagation speeds tend to imply small critical quenching diameters (i.e., $D_{crit.}$). Specifically, based on the values for propane and hexane shown in the figure, the methanol fuel/air mixture is anticipated to have a $D_{crit.}$ value on the order of 2.3 millimeters or greater.

Critical flame-quenching diameters

Fuel (U_L, m/s)*	D_{crit}, m
Hydrogen (3.1)	7×10^{-4}
Acetylene (1.6)	7×10^{-4}
Propane (0.45)	2.4×10^{-3}
***n*-Hexane** (0.45)	2.4×10^{-3}

* U_L is the laminar burn velocity.

Figure 72. Flame Quenching Diameters

This turns out to be well above the mean cross-sectional values that are currently used in the AFCT channel sizes, thus mitigating the risk of a flame front propagating through the heat sheet and into the vaporizer.

In addition, the insertion of metal mesh or screens anywhere in the feed-stream flow path can act as flame front extinguisher, as long as their mesh size is adjusted to be below $D_{crit.}$. Independent

of the $D_{crit.}$ value, the metal mesh will also tend to extinguish the flame by virtue of its thermal mass which absorbs energy.

A third mitigation strategy, separate from the ones mentioned above and inherent to AFCT technology, will further reduce the flammability hazard. This strategy is to make sure that the reactor never has more than a minuscule amount of chemical energy in residence at any time.

Thus, even if all other strategies were somehow to fail and the reactor contained a breach and it had greater than 6% fuel/air ratio within its channels and an ignition source were present, then the amount of chemical energy present at that moment would use itself up completely in a fraction of a second. This would happen because the air pump would be shut-off as a result of the reactor sheet detecting anomalous temperature excursions.

HAZARD #2: Toxicity

Methanol is known to be more toxic than ethanol. Toxicity effects for any substance are dose dependent. For methanol, lethal doses are dependent on body weight, but in general, an adult can survive ingesting up to 50 to 136 ml. Authorities advise that swallowing up to 1.3 grams or 1.7 ml of methanol or inhaling methanol vapor concentrations below 200 ppm should be harmless for most people. No severe effects have been reported in humans of methanol vapor exposures even well above 200 ppm. Sub-lethal amounts are possibly dangerous to health if ingested in the quantity of 10 ml or more. Methanol in even smaller doses is a natural component of the human body and can be found in the food we eat. Because of that, methanol is not thought to have any mutagenic or carcenogenic properties.

Ingesting even 10 ml is virtually impossible on an accidental basis if the methanol is denatured with a substance called Bitrex. Bitrex is so distasteful to humans and animals that it causes a spontaneous spitting reaction that prevents further ingestion. Again this is an unlikely event so long as Bitrex is employed as a denaturing agent. Typically Bitrex is deployed in doses of 10 ppm and, in itself, is not dangerous.

Nevertheless, active mitigation of the hazard can be obtained during the use of any CDI catalytic combustion product by incorporating specific features. These include providing a closed system whereby the exhaust products, including any unburned methanol vapor, is "scrubbed" before return to the environment. Scrubbing refers to the process of placing a chemical agent in the path of the exhaust stream which either absorbs chemically alters the offending components. This can be done using something as simple as activated charcoal.

Mishaps due to liquid fuel spillage is ameliorated by incorporating a design feature whereby the liquid fuel source is separated from reactor. This allow for implementing specific engineering regulations adopted by the world for all consumer products that will incorporate methanol based micro-fuel cells. In other words, the fuel cartridge approach is utilized instead of a refillable tank, thus allowing CDI to utilize all of the safety experience and approved engineering these standards have pioneered.

A mishap due to a break in the closed system is handled by detecting the resulting drop in system pressure and having the control electronics terminate the combustion process.

4. Conclusions

4.1 Summary of Technology Status

Over the course of the project, each of the three critical subsystems; (a) electronic control, (b) vaporization and metering, and (c) catalytic reactor (i.e., heat-sheet) were developed and adapted for a specific end use, an MRE heater.

Extensive testing and improvements in each subsystem resulted from this effort. More often than not, this required numerous variations in the original designs and parallel development paths aimed at exploring alternative technological approaches.

One subsystem in particular, the vaporization & metering, required the most resources and underwent the greatest evolution. Of the three approaches explored, the planar VEM approach appears to include the best characteristics for the intended application. It is also the most reliable and manufacturable design of the three explored in this project.

The catalytic reactor subsystem also underwent a number of variations. The chief challenges with this subsystem were in the areas of material compatibility and assembly compatibility. By "compatibility" is meant that the catalyst-coated heat elements are often sensitive to the severe outgassing and high local concentrations of volatile organic compounds that will naturally occur during the bonding, gluing, potting and general operation of the subsystem. The other area of challenge for this subsystem is in the manufacturability of the heat elements. A considerable effort was expended to achieve an element with consistent and repeatable properties.

The degree of complexity of the electronic control subsystem was dependent on the choice of vaporization and metering subsystem. The TIJ vaporization scheme required the most complexity and the VEM required the least.

The electronic control subsystem effort was far less problematic in terms of schedule delays and technical risk because a wide variety of state- of-the-art electronic control components already exist off-the-shelf. This allowed for a wide range of design options. In addition, electronic PCB and flex circuit fabrication services are readily available that allow for economic and rapid prototyping and a clear path to volume manufacture.

A variety of control techniques were explored based on CPLD's, FPGA's and MCU's. Ultimately, the MCU, with its advanced state of integrated "on-board" chip peripherals was the best choice as the core technology for the electronics. It allowed for ease and flexibility of programming and a high degree of miniaturization in the finished product.

4.2 Recommendations

Based on the data and experience with prototypes, as well as examining the feasibility of achieving a low cost and a volume-manufacturable product, the logical choice for vaporization and fuel metering would be the planar VEM. The planar VEM has an inherently high power

density (i.e., watts per unit device volume) when compared to either the TIJ or the catalytically driven capillary (i.e., ceramic wick) pump device.

The VEM and each of the other two vaporization devices are sub categories of the forced air evaporation (FAE) genus. Although CDI is the originator and patent holder of the passive form of catalytic combustion, sometimes known as membrane diffusive, the VEM approach has certain critical advantages that suggested that it should be the primary approach.

Table 3 delineates the most salient features of each category. A particularly important point shown in this table is that a "man-safe" rating is far easier to obtain with the VEM approach.

One of the reasons for this results from the fact that FAE devices can be constructed as a completely closed system, whereby the exhaust is returned to the vaporization unit and processed before release to the environment. So, no unburned byproducts can affect the users. In addition, the fuel/air ratio can be set well below flammability limits.

Another important feature of FAE is that liquid fuel never leaves the confines of a internationally certified cartridge (IEC specifications). To receive this rating means that under no reasonable foreseen condition (i.e., civilian use) can liquid methanol escape. This keeps the fuel source physically separate from the reactor and any other possible ignition source. The IEC engineering regulations for methanol have been adopted by the world for all consumer products that will incorporate methanol based micro-fuel cells. Micro-fuel cells and CDI's flameless technology have nearly identical safety profiles.

Table 3. Forced Air Evaporation versus Membrane Diffusive

Solution Sub-Type (Captive Catalytic Combustion)	Advantages	Disadvantages
1. Membrane Diffusive	• Simplified system design. • Lower potential cost. • Natural filtering of certain types of impurities to protect catalyst.	• Power output limited by natural processes. • Reaction products difficult to manage. • Difficult to obtain rapid on/off behavior. • Tends to lack precise temperature control. • "Man-Safe" certification issues
2. Forced Air	• High power output. • Rapid turn on/off. • Precise temperature control. • No combustible or toxic fluids near heated surfaces. • Reaction products collected and scrubbed. • Easier to certify "Man-Safe"	• Higher cost • More complex control/ regulation issues

This document reports research undertaken at the U.S. Army Natick Soldier Research, Development and Engineering Center, Natick, MA, and has been assigned No. NATICK/TR- 10/017 in a series of reports approved for publication.